3-27-2020

Loss of H3K36 methyltransferase SETD2 impairs V(D)J recombination during lymphoid development

S Haihua Chu
Dana Farber Cancer Institute

Putzer J Hung
Washington University School of Medicine in St. Louis

et al

iScience

CellPress

Article

Loss of H3K36 Methyltransferase SETD2 Impairs V(D)J Recombination during Lymphoid Development

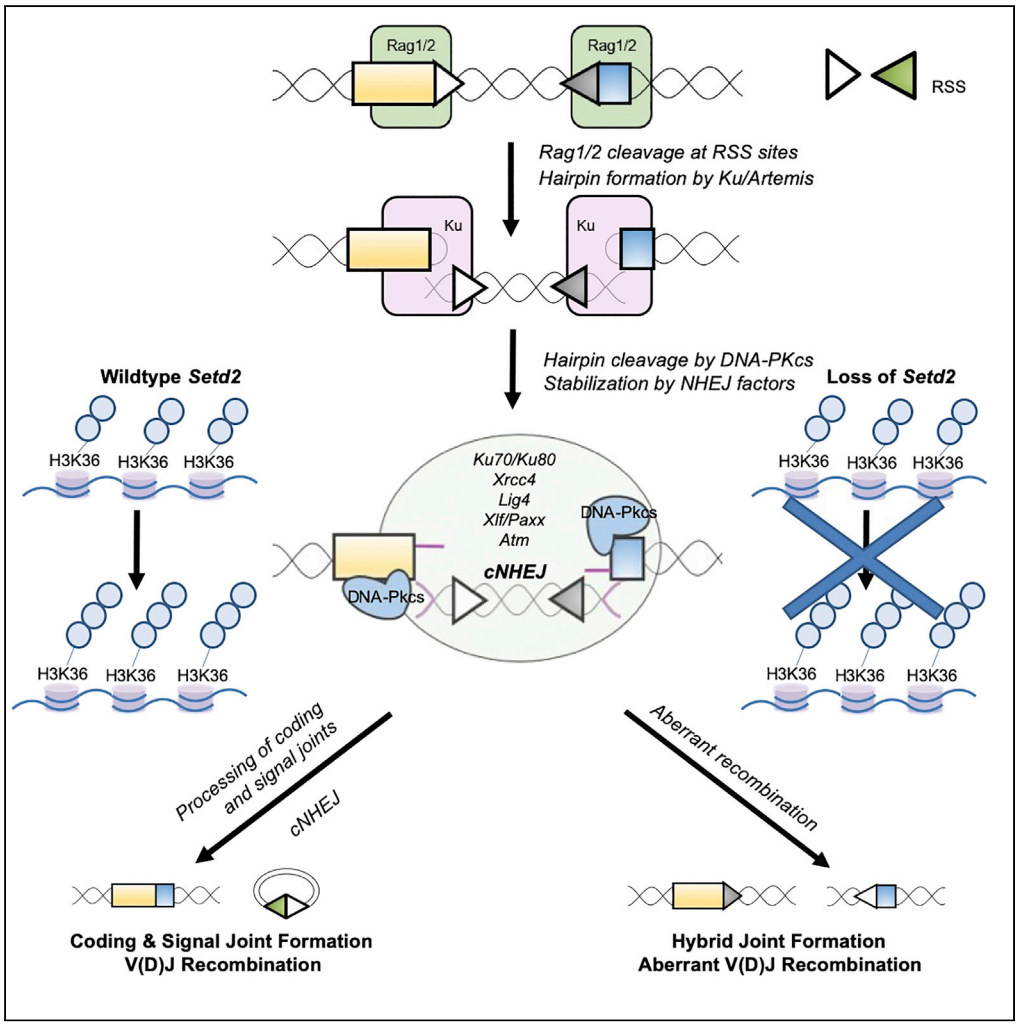

S. Haihua Chu, Jonathan R. Chabon, Chloe N. Matovina, ..., Andre Nussenzweig, Barry P. Sleckman, Scott A. Armstrong

scott_armstrong@dfci.harvard.edu

HIGHLIGHTS

Setd2/H3K36me3 is essential in maintaining a normal hematopoiesis

Loss of *Setd2*/H3K36me3 impairs lymphogenesis and V(D)J recombination

Loss of *Setd2*/H3K36me3 and ATM kinase activity leads to mis-repaired recombination

Setd2/H3K36me3 prevents apoptosis of post-mitotic neuronal cells

DATA AND CODE AVAILABILITY

GSE130904
GSE131588
GSE131608
GSE131690

Chu et al., iScience *23*, 100941 March 27, 2020
https://doi.org/10.1016/j.isci.2020.100941

iScience

CellPress

Article

Loss of H3K36 Methyltransferase SETD2 Impairs V(D)J Recombination during Lymphoid Development

S. Haihua Chu,[1] Jonathan R. Chabon,[1] Chloe N. Matovina,[1] Janna C. Minehart,[2] Bo-Ruei Chen,[3] Jian Zhang,[4,5] Vipul Kumar,[6,7] Yijun Xiong,[1] Elsa Callen,[8] Putzer J. Hung,[3,9] Zhaohui Feng,[1] Richard P. Koche,[10] X. Shirley Liu,[5] Jayanta Chaudhuri,[11,12] Andre Nussenzweig,[8] Barry P. Sleckman,[3] and Scott A. Armstrong[1,13,*]

SUMMARY

Repair of DNA double-stranded breaks (DSBs) during lymphocyte development is essential for V(D)J recombination and forms the basis of immunoglobulin variable region diversity. Understanding of this process in lymphogenesis has historically been centered on the study of RAG1/2 recombinases and a set of classical non-homologous end-joining factors. Much less has been reported regarding the role of chromatin modifications on this process. Here, we show a role for the non-redundant histone H3 lysine methyltransferase, *Setd2*, and its modification of lysine-36 trimethylation (H3K36me3), in the processing and joining of DNA ends during V(D)J recombination. Loss leads to mis-repair of Rag-induced DNA DSBs, especially when combined with loss of Atm kinase activity. Furthermore, loss reduces immune repertoire and a severe block in lymphogenesis as well as causes post-mitotic neuronal apoptosis. Together, these studies are suggestive of an important role of *Setd2*/H3K36me3 in these two mammalian developmental processes that are influenced by double-stranded break repair.

INTRODUCTION

In early normal lymphocyte development, gene segments that will eventually encode the immunoglobulin (Ig) and T cell receptor (TCR) variable regions are recombined from Variable (V), Diversity (D), and Joining (J) gene segments in a process known as V(D)J recombination (Alt et al., 2013). During the DNA recognition and cleavage stage, recombination signal sequences (RSSs) that flank the individual V, D, and J gene segments are targets of RAG1/2 endonucleases and result in the generation of hairpinned coding ends (CEs) and blunt-ended signal ends (SEs) (Alt et al., 2013; Schatz and Swanson, 2001). In the second phase of V(D)J recombination, and-processing and end-ligation of CEs and SEs are mediated by classical non-homologous end-joining (C-NHEJ) factors and produce an imprecisely repaired coding joint (CJ) consisting of V(D)J exons and a precisely repaired but discarded circular signal joint (SJ) (Alt et al., 2013; Schatz and Swanson, 2001). A set of core C-NHEJ factors (KU70, KU80, XRCC4, and LIG4) is absolutely essential for end-joining and is evolutionarily conserved (Alt et al., 2013; Kumar et al., 2014). Loss or defects of C-NHEJ factors can impair end-processing (DNA-PKCs, ARTEMIS) or end-joining (KU proteins, XRCC4, XLF, LIG4) and results in severe immunodeficiencies in both mouse models and human disease (Alt et al., 2013; Kumar et al., 2014; Bassing et al., 2002). The DNA damage protein, ataxia telangiectasia mutated (ATM); its target, histone H2AX; and DNA damage response adaptor protein, MRI, are all also involved in the end-ligation process (Bredemeyer et al., 2006; Yin et al., 2009; Hung et al., 2018). The single loss of any of these factors, or C-NHEJ factor XLF, has only modest effects on lymphogenesis and V(D)J recombination (Bredemeyer et al., 2006; Yin et al., 2009; Hung et al., 2018; Li et al., 2008). In addition to loss of the core C-NHEJ factors, combined deficiencies of proteins non-essential for the end-joining reaction can severely impair C-NHEJ to a similar extent, as in the case of combined loss of Xlf and Atm or Xlf and Mri (Kumar et al., 2016; Hung et al., 2018; Li et al., 2008; Lescale et al., 2016; Zha et al., 2011).

Another mammalian developmental process that utilizes C-NHEJ for repair of double-strand breaks (DSBs) is embryonic neurogenesis (Frappart and McKinnon, 2008). Neural progenitors that have exited the cell cycle and are migrating out of the embryonic ventricular zones as they differentiate are thought to rely on NHEJ-mediated repair of DSBs (Frappart and McKinnon, 2008). In mice, loss of core C-NHEJ factors leads to apoptosis of post-mitotic neurons and embryonic lethality (Gao et al., 1998; Frank et al., 2000; Gu et al.,

[1]Department of Pediatric Oncology, Dana Farber Cancer Institute, and Division of Hematology/Oncology, Boston Children's Hospital, 450 Brookline Avenue, Boston, MA 02215-5450, USA

[2]New York University School of Medicine, New York, NY, USA

[3]Department of Pathology and Laboratory Medicine, Weill Cornell Medical College, New York, NY, USA

[4]Center for Computational Biology, Beijing Institute of Basic Medical Sciences, Beijing, China

[5]Department of Biostatistics and Computational Biology, Dana-Farber Cancer Institute and Harvard T.H. Chan School of Public Health, Boston, MA, USA

[6]Howard Hughes Medical Institute, Department of Pediatrics, Department of Genetics, Harvard Medical School, Boston, MA, USA

[7]Harvard-MIT MD-PhD Program, Harvard Medical School, Boston, MA, USA

[8]Laboratory of Genome Integrity, National Cancer Institute National Institutes of Health, Bethesda, MD, USA

[9]Department of Pathology and Immunology, Washington University School of Medicine, St. Louis, MO, USA

[10]Cancer Biology and Genetics, Memorial Sloan Kettering Cancer Center, New York, NY, USA

[11]Immunology Program, Memorial Sloan Kettering Cancer Center, New York, NY, USA

Continued

2000). Moreover, the same synthetic lethal combinations that result in severe lymphocyte developmental blocks (e.g., MRI and XLF) also display similar post-mitotic neuronal apoptosis (Hung et al., 2018; Abramowski et al., 2018), indicating the critical role of end-ligation and C-NHEJ in the repair of DSBs during neurogenesis.

Histone H3 lysine-36 tri-methylation (H3K36me3) is a histone modification that is catalyzed by the non-redundant histone methyltransferase, *SETD2* (Wagner and Carpenter, 2012). H3K36me3 is associated with actively transcribed genes, and *SETD2* plays important roles in the control of gene expression (Wagner and Carpenter, 2012). Loss-of-function mutations in *SETD2* or dominant negative "onco-histone" mutations in the H3K36 residue itself have been described in a broad array of malignancies, particularly in hematopoietic and central nervous system (CNS) tumors (Parker et al., 2016; Zhang et al., 2012; McKinney et al., 2017; Moffitt et al., 2017; Zhu et al., 2014; Lu et al., 2016). In mammalian cells, *SETD2* regulates specific steps of the DNA damage response during mismatch repair (MMR) and homologous recombination (HR) (Li et al., 2013; Pfister et al., 2014; Aymard et al., 2014). More recently, a role for *Setd2* in normal thymocyte development and V(D)J recombination was described (Ji et al., 2019). Although a role for H3K36 methylation in NHEJ had been previously suggested in yeast (Fnu et al., 2011), insights into the mechanism for how this post-translation histone modification in mammalian cells may impact this mode of repair remains unknown. Thus, to determine the role, if any, of *Setd2* and H3K36me3 in this mode of DNA repair in mammals, we studied its loss in two developmental pathways that utilize NHEJ. Here, we specifically show that whereas loss of *Setd2*/H3K36me3 does not completely abrogate repair of DSBs, loss leads to mis-repair in B-cell lymphoid development of Rag-induced DNA DSBs, especially when combined with loss of ATM kinase activity. Loss of *Setd2* leads to the increased formation of aberrant hybrid joints and additionally leads to reductions in overall B cell repertoire. Finally, loss of *Setd2* also leads to post-mitotic neuronal apoptosis.

RESULTS

Loss of *Setd2* Disrupts Normal Hematopoiesis, Particularly Lymphopoiesis

The complete loss of *Setd2* is embryonic lethal at embryonic day 10.5 (E10.5)–E11.5 (Hu et al., 2010). Therefore, to study the role of *Setd2* in normal and malignant hematopoiesis, we previously generated a conditional mouse model expressing *Cre*-recombinase under inducible (*Mx1*) or constitutive (*Vav1*) hematopoietic lineage-restricted promoters (Mar et al., 2017). The loss of *Setd2* ablated H3K36me3 in hematopoietic tissues through excision of exon 3 of *Setd2* (Figure 1A). Heterozygous mice had no overt hematopoietic phenotype (Figures S1A, S1B and S2D), whereas homozygous loss of *Setd2* resulted in a significant perturbation of normal hematopoiesis, including decreased overall bone marrow cellularity (Figure 1B), significant loss of mature lymphoid cells ($B220^+$ B cells and $CD3^+$ T cells) in the bone marrow, and expansion of erythroid ($Ter119^+$) cells (Figures 1C and 1D). The significant reduction in T cells in the bone marrow observed upon complete *Setd2* loss was also mirrored by a severe diminution of thymic size (Figure 1E), which was concomitant with significant splenomegaly (Figure 1F). Strikingly, the splenomegaly was due to the aberrant expansion of erythroid cells and significant ablation of B-lymphoid ($B220^+$) populations (Figure 1G). In addition, loss of *Setd2* induced qualitative and quantitative defects in hematopoietic stem cells, as well as abnormal erythroid progenitor expansion in the bone marrow (Figures 1D, 1G, 1H, S1C–S1F, and S2A–S2C). These hematopoietic phenotypes are consistent with other reports on *Setd2* knockout mice (Zhou et al., 2018; Zhang et al., 2018; Ji et al., 2019). Altogether, these data indicate that loss of *Setd2* disrupts normal hematopoiesis and severely impacts lymphoid development.

Setd2/H3K36me3 Is Important in Normal Lymphocyte Development

We and others (Zhou et al., 2018; Zhang et al., 2018; Ji et al., 2019) observed that loss of *Setd2* early in hematopoiesis resulted in significant depletions of the lymphoid populations in the bone marrow, spleen, and thymus (Figures 1C, 1D, 1G and S1). To rule out that these early developmental deficiencies were not solely the result of reduced numbers of early lymphoid progenitors (Figure S1C), we crossed our knockout mice with multiple B lymphoid lineage-restricted *Cre*-recombinase-expressing lines and found that whereas an early and profound proB block in development was only observed upon early deletion of *Setd2* (*Mx1, Vav1cre*) (Figure 2A), the deletion of *Setd2* in later stages of B cell development (with *hCD2, Mb1,* and *Cd19*cre) resulted in abnormal lymphocytic output that was more apparent in more mature B cell populations (Figures 2B and 2C). Specifically, loss of *Setd2* induced at later stages of B cell development significantly reduced detectable mature B cells (IgM^+IgD^+) in the bone marrow (Figures 2B and 2C) and resulted in the significant depletion of B cell lineage cells in the spleen (Figure 2C). These data

[12]Immunology and Microbial Pathogenesis Program, Weill Cornell Graduate School of Medical Sciences, New York, NY, USA

[13]Lead Contact

*Correspondence: scott_armstrong@dfci.harvard.edu

https://doi.org/10.1016/j.isci.2020.100941

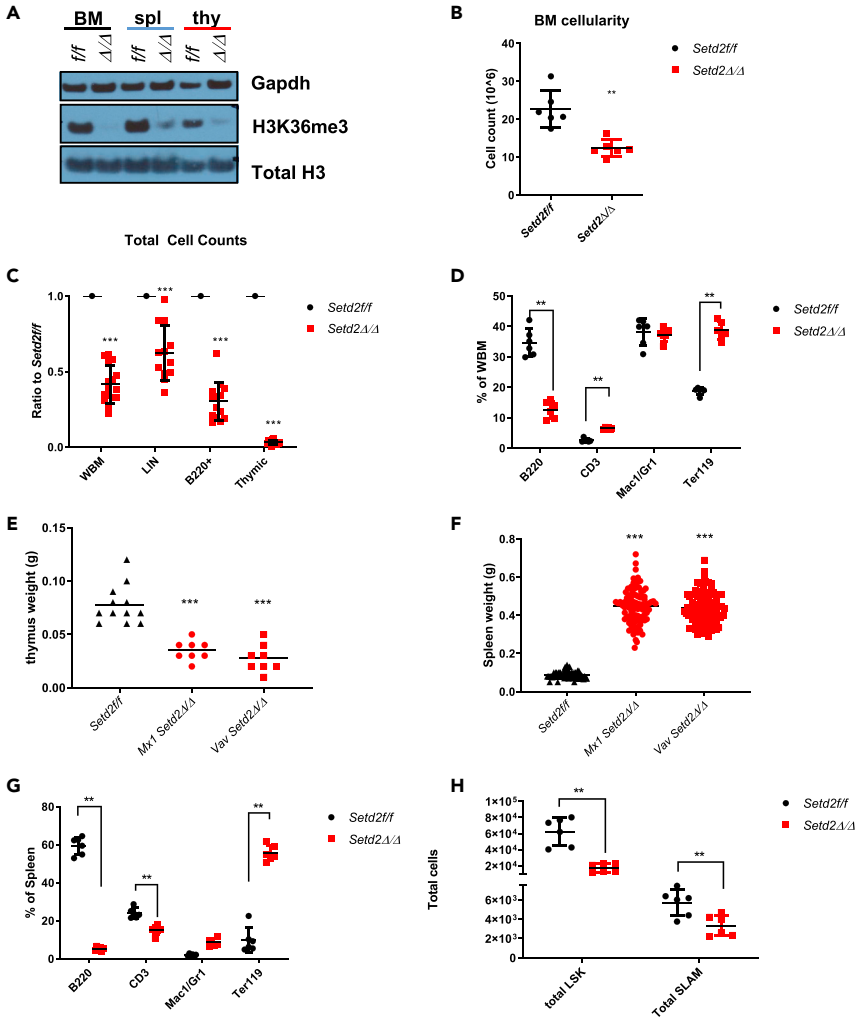

Figure 1. Loss of *Setd2*/H3K36me3 Disrupts Normal Hematopoiesis and Severely Arrests Lymphoid Development

(A) Western blot for H3K36me3, total H3, and Gapdh in bone marrow (BM), spleen (spl), and thymus (thy) of *Mx1/Vav1cre Setd2Δ/Δ* and *Setd2f/f* littermate controls.

(B) Total cell count of whole bone marrow (n = 6 for all groups).

(C) Ratio of *Mx1* and *Vav1 Setd2Δ/Δ* to controls of total cellularity of whole bone marrow (WBM), lineage-negative bone marrow cells (LIN^-), $B220^+$ B cells in bone marrow, and thymocytes (n = 15 for all groups).

(D) Percent composition of differentiated hematopoietic cell populations in WBM, B cell ($B220^+$), T cell ($Cd3^+$), myeloid ($Mac1^+/Gr1^+$), and erythroid ($Ter119^+$) (n=6 for all groups).

(E) Thymic (n = 10) and (F) spleen (n = 100) weights for *Setd2Δ/Δ* and *Setd2f/f* littermate controls.

(G) Percent composition of differentiated hematopoietic cell populations in spleen.

(H) Total cellularity of LSK ($Lin^-Sca1^+Kit^+$) and SLAM (LSK $Cd150^+Cd48^-$) hematopoietic stem populations (n = 6 for all groups).

**, $p < 0.01$ ***, $p < 0.001$. See also Figures S1 and S2.

suggest that *Setd2*/H3K36me3 is important in B lymphopoiesis at different stages, but that the severe block at the proB cell stage was only apparent with early loss in hematopoiesis.

Setd2/H3K36me3 Is Crucial for Normal Immunoglobulin Rearrangement in Early Lymphocyte Development Recombination

The severe block in early B cell development was striking and warranted further examination. Early loss of *Setd2*/H3K36me3 blocked B cell development at the proB cell stage with similar total numbers of Fraction A (FrA)-defined pre-proB cells when compared with littermate controls (Figures 3A and S3A–S3E). This block at the

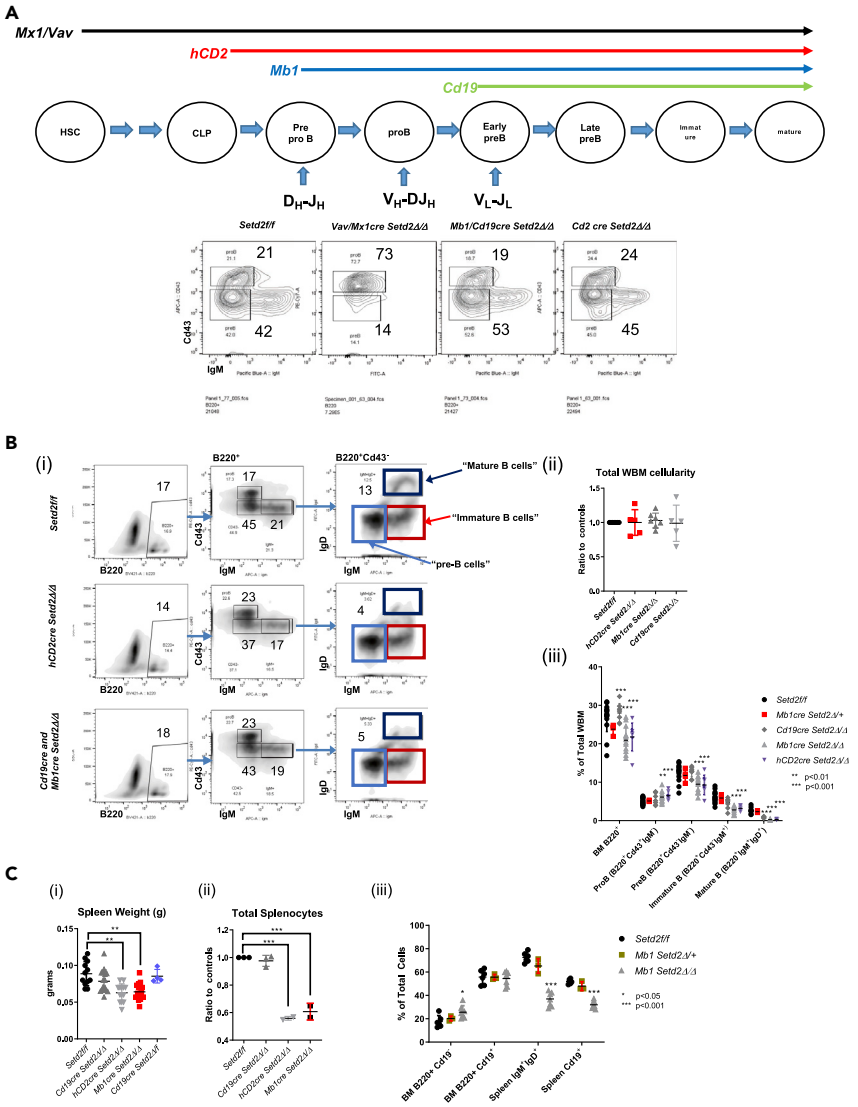

Figure 2. *Setd2*/H3K36me3 Important for B Cell Development at Different Stages

(A) Schematic of ontological expression of various B-lineage-restricted *cre*-recombinase mouse lines crossed to *Setd2f/f* mice with Igh locus rearrangement status indicated, and representative flow cytometry of $B220^+$ early B cells progenitors (proB and preB cells) of control, *Vav/Mx1, hCD2, Cd19, and Mb1cre Setd2Δ/Δ* mice.

(B) (i) Representative flow cytometry of bone marrow stained for early B cell progenitors and mature and immature B cell markers (IgM and IgD). (ii) Total bone marrow cellularity. (iii) Fraction composition of $B220^+$, proB ($B220^+Cd43^+IgM^-$), preB ($B220^+Cd43^+IgM^-$), immature B ($B220^+Cd43^+IgM^+$), and mature B cell ($B220^+IgM^+IgD^+$) populations of *hCD2* (n = 7), *Mb1* (n = 14), *Cd19* (n = 9) *Setd2Δ/Δ*, and sex- and age-matched littermate controls.

(C) Spleen (i) weight (n = 14 for all groups), (ii) total cellularity (n = 3 for all groups), and (iii) percentage composition of different B cell populations in bone marrow and spleen (n = 6 for all groups).

Significance indicated as comparison with controls. *p < 0.05, **p < 0.01, ***p < 0.001, error bars represent SD.

proB cell stage was concomitant with a near-complete ablation of immature IgM^+ B cells in the bone marrow and spleen (Figures 3A and S3B). Similarly, *Setd2Δ/Δ* mice exhibited a block in early T cell development at the double-negative stage (DN: $CD4^-CD8^-$), with an accumulation at the DN3 stage (Figure 3B). This arrest at the DN3 stage was similarly observed in *Mx1*-cre-driven exon 6-7 deletion *Setd2* knockout mouse (Ji, et al., 2019). Thus, lymphopoiesis in *Setd2Δ/Δ* mice appeared to be arrested at stages wherein V(D)J recombination occurs and is reminiscent of the lymphopenia observed with deficiency of factors necessary for V(D)J recombination (Alt et al., 2013; Kumar et al., 2014; Bassing et al., 2002). In all early B/T cell progenitor populations of *Setd2Δ/Δ* mice, developmental blocks also coincided with increased levels of apoptosis and phospho-γH2ax (Figures 3C, S3F, and S3G),

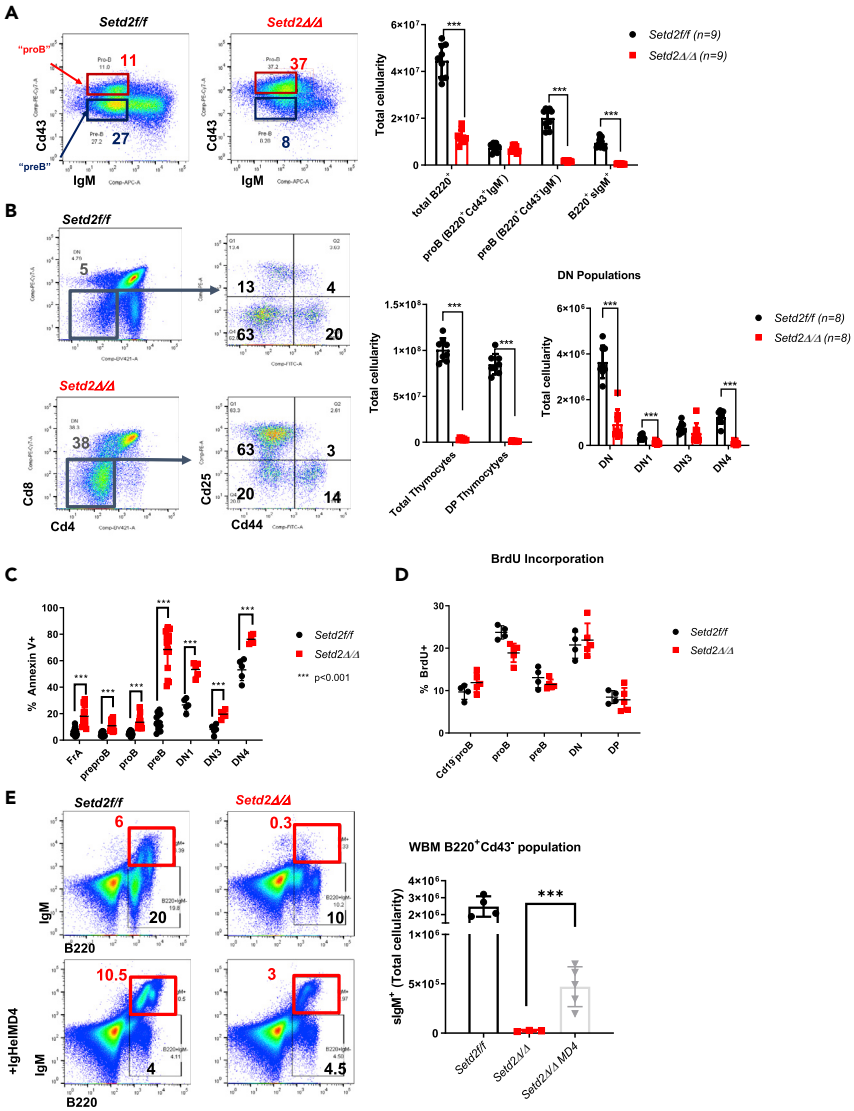

Figure 3. Loss of *Setd2*/H3K36me3 Severely Arrests Lymphoid Development

(A) Representative flow cytometry analysis of early B cell progenitors in B220$^+$ bone marrow and total cellularity of B cell progenitor proportions of *Vav/Mx1cre Setd2Δ/Δ* and controls (n = 9).

(B) Representative flow cytometric analysis of thymic cells, and total cellularity of thymic progenitor populations in *Setd2Δ/Δ* and *Setd2f/f* controls. DN: Cd4$^-$Cd8$^-$, DN1: DN Cd44$^+$Cd25$^-$; DN2: DN Cd44$^+$Cd25$^+$; DN3: DN Cd44$^-$Cd25$^+$ (n = 8).

(C) Annexin V$^+$ of B (n = 9) and T cell (n = 5) progenitor populations.

(D) *In vivo* bromodeoxyuridine (BrdU) incorporation in early B and T cell progenitor compartments (n = 3). All values for BrdU were non-significant.

(E) Representative immature B cell (B220$^+$sIgM$^+$) flow cytometric analysis and total cellularity of immature surface IgM$^+$ population of bone marrow cells isolated from both legs and hips of *Setd2* mice crossed to mice transgenic for the Ig heavy chain complex (IgHelMD4) specific for hen egg lysozyme (HEL) (n = 4 for *Setd2f/f*, n = 5 for *Setd2Δ/Δ* MD4, and n = 3 for *Setd2Δ/Δ*).

*** p<0.001, error bars represent SD. See also Figures S3 and S4.

despite similar *in vivo* proliferation rates and cell cycle status (Figures 3D and S3H). Furthermore, *Setd2Δ/Δ* proB cells did not display any significant differences in the expression of factors related to V(D)J recombination at the gene or protein level (Figures S4A–S4C). The arrest in B cell, but not in T cell, development in *Setd2Δ/Δ* mice could be partially rescued by crossing knockout mice with a transgenic mouse expressing a fully rearranged

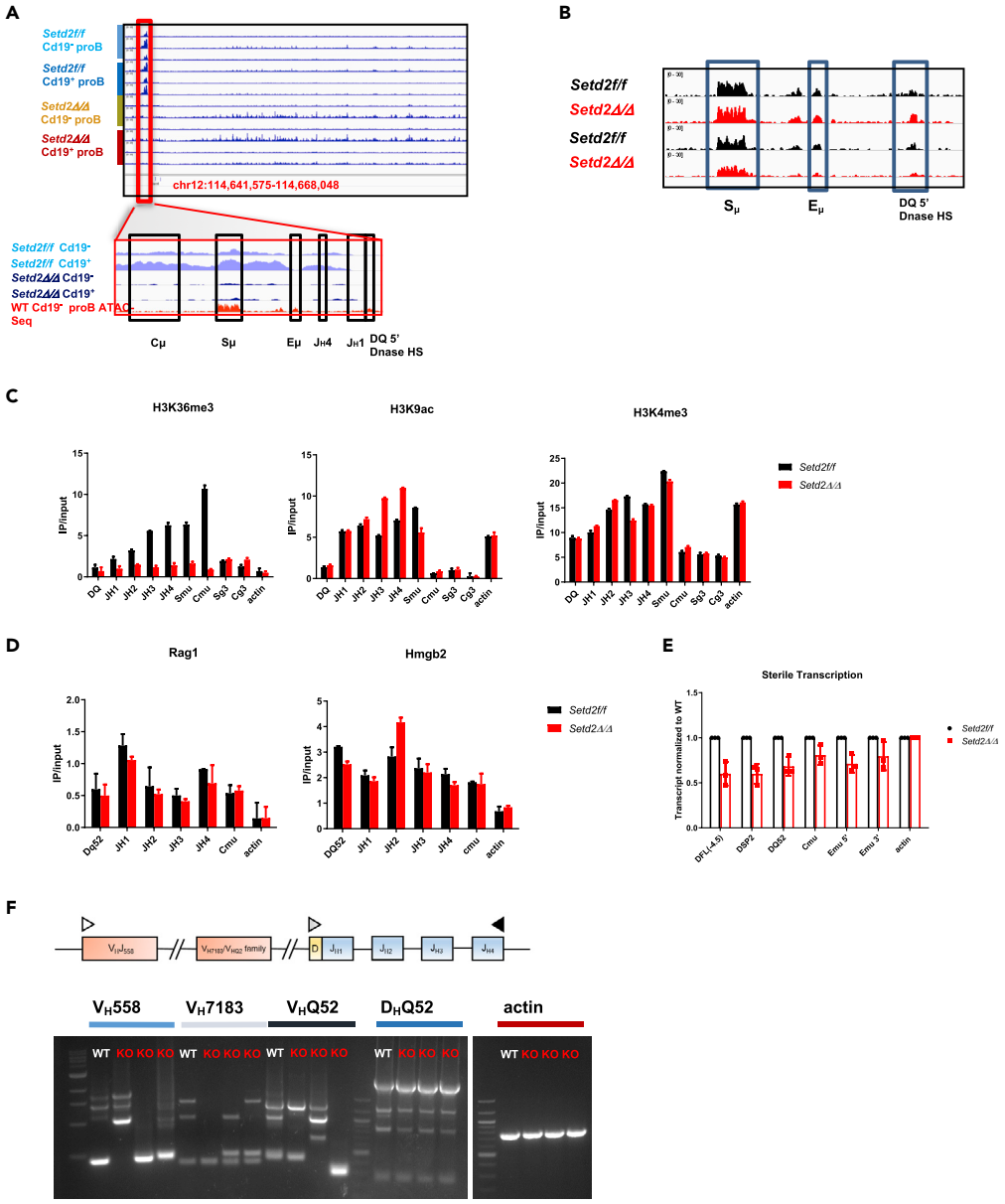

Figure 4. Loss of *Setd2*/H3K36me3 Does Not Alter Chromatin Architecture or Accessibility of the Early proB Igh Locus and Causes Abnormal V(D)J Recombination

(A) H3K36me3 ChIP sequencing of the Igh locus of Cd19$^{-/+}$ proB (B220^{+}Cd43^{+}IgM^{-}) cells from bone marrow of *Vav Setd2Δ/Δ* and controls. (n = 3 for all groups). Magnification of region of Igh with focal H3K36me3; loss of representative H3K36me3 tracks overlaid with assay for transposase-accessible chromatin (ATAC)-seq of same region from control proB cells for reference. Annotation of critical regulatory sites as indicated.

(B) Representative ATAC-seq tracks of regulatory region of the Igh locus described in (A) of sorted Cd19^{-} proB cells from two matched control and *Setd2* knockout sorted proB cells.

(C) Representative ChIP-PCR of regulatory region for histone H3 marks K36me3, K9ac, and K4me3. Data representative of n = 3 independent experiments.

(D) Representative ChIP-PCR of Rag1 and Hmgb2 of proB cells from *Setd2Δ/Δ* and controls at the same regulatory region with standard deviations as indicated, n = 3 independent experiments.

(E) Relative quantitation of sterile transcription of D_H genes, Cμ, and enhancer RNAs of proB cells from *Setd2Δ/Δ* and controls. Data represented as an average of three independent ChIP-PCRs from three independently sorted proB cell populations.

Figure 4. *Continued*

(F) Schematic and representative results of PCR assay to detect V(D)J recombination products of rearrangement of the Igh locus of different V_H families of sorted proB cells from *Setd2Δ/Δ* (KO) and controls (WT). Empty and filled triangles represent primers. No product meant germline non-rearrangement. Image representative of n = 3 independent PCR experiments.

Error bars represent SD. See also Figure S5.

and productive immunoglobulin heavy chain (Igh) locus (Figure 3E), indicating a role for *Setd2*/H3K36me3 in enforcing normal V(D)J recombination.

Loss of *Setd2*/H3K36me3 Does Not Abrogate Chromatin Architecture or Accessibility of the Early proB Igh Locus and Causes Aberrant V(D)J Recombination

To determine the impact of loss of *Setd2*/H3K36me3 on the Igh locus at the proB stage, we conducted chromatin immunoprecipitation (ChIP) sequencing and found both a global loss of H3K36me3 across the genome and a focal loss on the Igh locus where a well-studied critical regulatory region near the Eμ enhancer resides (Chowdhury and Sen, 2001) (Figures 4A and S5A). As accessibility of this region is critical for B cell development (Chowdhury and Sen, 2001; Chakraborty et al., 2009), we wanted to ascertain if the loss of H3K36me3 affected local chromatin architecture or accessibility. In proB cells, ablation of H3K36me3 neither affected chromatin accessibility (Figures 4B and S5B) nor disrupted the local levels of H3K4me3 and H3K9ac (Figure 4C), two histone modifications essential for maintaining an open and actively transcribed chromatin structure at this regulatory region (Chowdhury and Sen, 2001; Chakraborty et al., 2009) and for H3K4me3, the recruitment and activation of the Rag2 protein itself (Shimazaki and Lieber, 2014; Johnson et al., 2010; Ji et al., 2010; Matheson and Corcoran, 2012; Bettridge et al., 2017). Loss of H3K36me3 did not significantly affect the methylation states of mono-, di-, or tri-methyl lysine-27 or mono- and di-methyl lysine-36 residues in this region (Figure S5C). We detected equivalent recruitment of Rag1 and Hmgb2 to this same region on the Igh locus (Shimazaki and Lieber, 2014; Johnson et al., 2010; Ji et al., 2010; Matheson and Corcoran, 2012) (Figure 4D), suggesting that the initiation phase of the V(D)J recombination reaction was intact. We were also not able to detect in sorted FrA proB cells any evidence of Rag1 recruitment or H3K36me3 at variable gene families on the Igh locus in either *Setd2*-deficient cells or controls (Figure S5D). In addition, the level of sterile transcription of Igh genes was only mildly reduced (Figure 4E), particularly when compared with deletion of the Eμ enhancer, which causes significant transcriptional dysregulation (Chakraborty et al., 2009). Upon closer examination of recovered V(D)J recombination products from proB cells, we observed that *Setd2* deficiency resulted in aberrant recombination and, in some cases, lack of expected rearrangement products altogether (Figures 4F and S5E). Combined, these data are suggestive that the V(D)J recombination defect is not due to decreased expression or regulation of the Igh locus, but due to defects in the repair phase of the reaction.

Aberrant End-Joining of Rag-Induced DSB with *Setd2*/H3K36me3 Deficiency

To ascertain if defects in *Setd2*-deficient lymphogenesis could be a consequence of impaired Rag-induced DSB repair during V(D)J recombination, we generated murine *Setd2*-deficient (*Setd2*$^{-/-}$), *Ku80*$^{-/-}$ (*Xrcc5*$^{-/-}$), *and Lig4* $^{-/-}$ late-proB v-Abelson (v-Abl)-transformed lines expressing a *Bcl2* transgene by CRISPR/Cas9-mediated inactivation (Figures S6A–S6D) (Hung et al., 2018; Jacobsen et al., 2006). Loss of *Setd2* in v-Abl cells neither perturbed the expression of factors involved in V(D)J recombination nor affected the cell cycle distribution of these cells (Figures S7A–S7C) *in vitro*. Treatment with Abl kinase inhibitor imatinib (STI) induces G1 cell-cycle arrest and *Rag1/2* expression leading to κ light chain rearrangement (Hung et al., 2018; Jacobsen et al., 2006) (Figure S8A). We additionally introduced a chromosomally integrated inversion recombination substrate (pMG-INV), which can be used to assess the efficiency of V(D)J recombination by measuring GFP expression in cells and/or visualization of the repair products and intermediates by Southern blotting and PCR-based strategies (Hung et al., 2018) (Figure 5A). Inactivation of ATM kinase activity with an inhibitor (ATMi) is sufficient to induce the formation of hybrid joints (HJs, joining of CEs to SEs) (Bredemeyer et al., 2006) and could additionally be used to observe aberrant V(D)J recombination.

Comparable rearrangement efficiency of the pMG-INV substrate was observed in both wild-type (WT) and *Setd2*$^{-/-}$ v-Abl cells treated with imatinib, as indicated by GFP expression (Figure 5B). As expected, treatment of WT v-Abl cells with ATMi resulted in a modest (25%) decrement in GFP expression (Figure 5B). Strikingly, treatment of *Setd2*$^{-/-}$ cell lines with ATMi resulted in a ~60% reduction in GFP expression (Figure 5C). This finding is reminiscent of the severe defect in GFP expression found in Xlf-deficient v-Abl cells

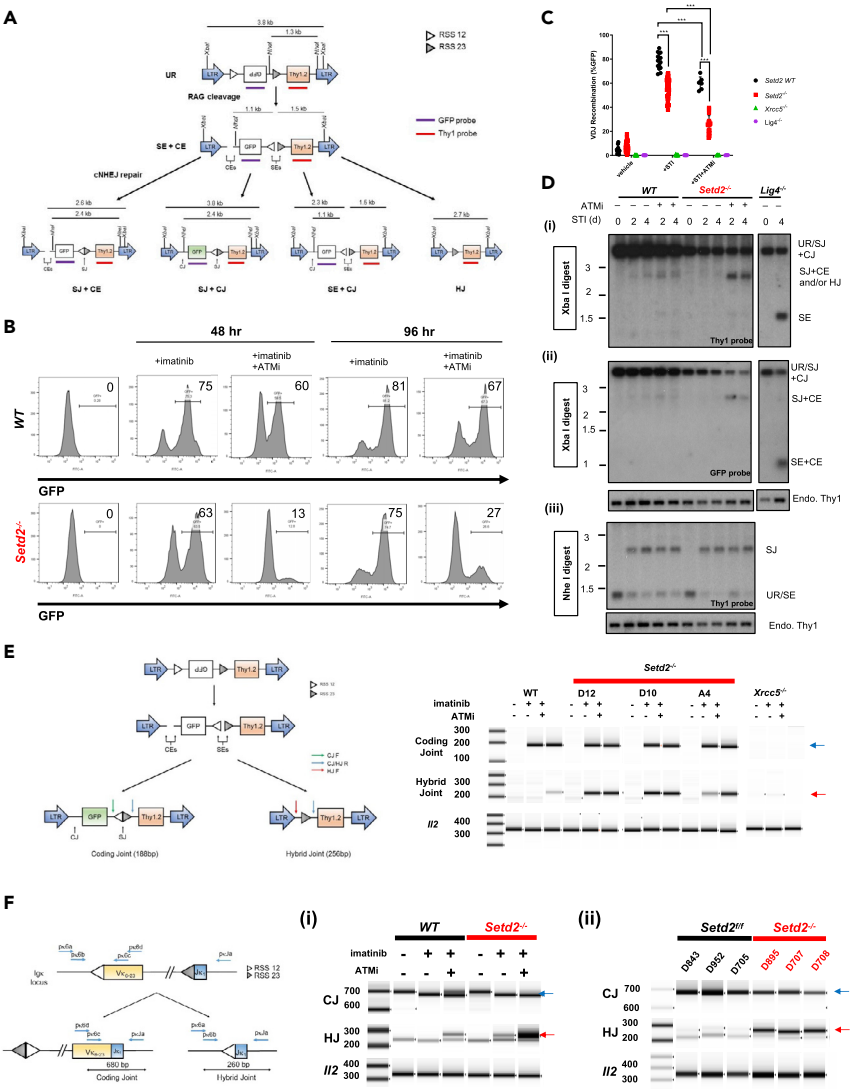

Figure 5. Aberrant End-Joining of Rag-Induced DSB with *Setd2*/H3K36me3 Deficiency

(A) Schematic of recombination substrate pMG-INV. Unrearranged (UR) and SE and CE intermediates and resulting SJs and CJs. Long-terminal repeats (LTRs), *XbaI* and *NheI* restriction digestion sites, recombination signal sequences (RSSs), GFP, *Thy1.2* cDNA, and corresponding probes shown.

(B) Representative flow cytometric analysis of GFP expression in control and *Setd2*$^{-/-}$ pMG-INV v-Abl cells treated with Abl kinase inhibitor imatinib (STI-571) and ATM kinase inhibitor (ATMi, KU55933) for 48 and 96 h.

(C) GFP expression of pMG-INV harboring v-Abl cell lines treated for 72 h with imatinib ± ATMi assessed by flow cytometry. Control, *Lig4*$^{-/-}$, and at least four independently derived *Xrcc5*$^{-/-}$ and *Setd2*$^{-/-}$ v-Abl clones were treated in n = 4 independent induction experiments. Significance to controls to STI-571 treatment alone condition was calculated. ***p < 0.001, error bars represent SD.

(D) Southern blot analysis of genomic DNA from induced *Setd2*$^{-/-}$ and control lines that were digested with (i and ii) XbaI and (iii) NheI hybridized with (i and iii) Thy1 or (ii) GFP probe. Hybrid Joins (HJ) indicated as well (joint of CEs and SEs).

(E) Schematic of PCR method to detect the formation of a coding joint and hybrid joint recombination product of the pMG-INV retroviral recombination substrate, and PCR result of pMG-INV coding and hybrid joints from indicated v-Abl cell clones treated for 72 h with ABLki with or without ATMki (KU55933). *Il-2* gene PCR was used as a loading control. Blue arrow indicates coding joint product, and red arrow indicates hybrid joint product.

(F) PCR strategy to detect endogenous Vκ6-23 to Jκ1 coding joints (CJ) and hybrid joints (HJ) in (i) control and *Setd2*-deficient v-Abl lines treated for 72 h with STI-571 ± ATMi and (ii) *Setd2f/f* and *Setd2Δ/Δ* splenocytes. *Il-2* gene PCR was used as a loading control and analyzed and quantified by high-sensitivity TapeStation (D1000). Blue arrow indicates CJ product, and red arrow indicates HJ product.

See also Figures S6–S9.

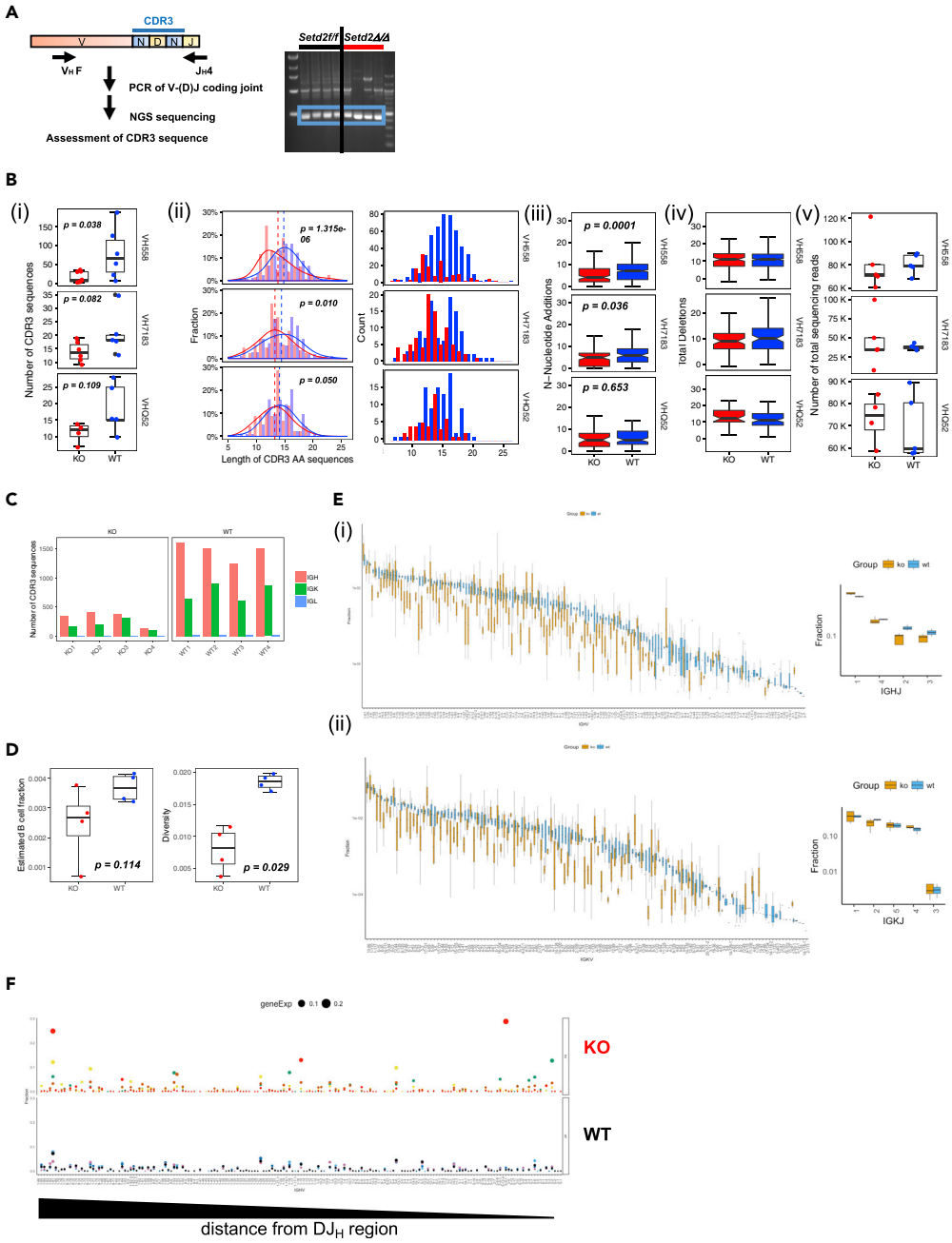

Figure 6. Loss of *Setd2*/H3K36me3 Reduces CDR3 Repertoire and Variable Gene Usage in proB Cells

(A) PCR and next-generation sequencing (NGS) strategy of V(D)J recombination products of V_H families to J_H4; 500-bp product (blue box) was extracted and submitted for NGS amplicon sequencing. Sequencing was analyzed with MiXCR T/B cell repertoire software (Bolotin et al., 2017).

(B) (i) Number of unique CDR3 clones, (ii) fraction and total clone counts by amino acid length, (iii) number of N-nucleotide additions, (iv) total nucleotide deletions of CDR3s recovered, and (v) total sequencing reads of *Setd2Δ/Δ* (KO) and controls for each V_H family. proB cells were sorted from n = 4 for each genotype and subjected to NGS analysis. Significance measured by Wilcoxon rank-sum test.

RNA sequencing analysis of four independently sorted control and four *Setd2Δ/Δ* proB cell compartments was also conducted, and *de novo* assembly of CDR3 sequences was conducted using the TRUST algorithm (Li et al., 2017; Hu et al., 2018, 2019). (C) Unique CDR3 counts for heavy and light chain Ig loci from TRUST analysis.

(D) Estimated B cell fraction of reads and B cell diversity recovered from analysis of RNA transcripts from TRUST analysis. Estimate B cell fraction was calculated by taking the fraction of number of reads mapped to BCR(IGV/IGJ/IGC) region to

Figure 6. *Continued*

total read count. B cell diversity was calculated by determining the ratio of unique CDR3 count over the total number of reads mapped to BCR region.

(E) Variable (V) and Joining (J) gene usage for (i) heavy chain and (ii) kappa light chain from TRUST analysis. Boxplots with SD.

(F) Clonality of CDR3s plotted as a fraction of total reads and ordered by individual Variable gene families and distance from Diversity (D) and Joining gene loci from most proximal to most distal from right to left from TRUST analysis. Relative size of clone indicated by size of dot.

treated with ATMi (Zha et al., 2011; Lescale et al., 2016) and suggests a functional redundancy between *Setd2*/H3K36me3 and Atm kinase activity in ensuring proper repair. To investigate potential effects on repair, we conducted Southern blotting, which revealed pMG-INV SJ and CJ formation without obvious accumulation of free unrepaired SEs and CEs in STI-treated WT and *Setd2*$^{-/-}$ v-Abl B cells (Figures 5D and S8B). Thus, like *Xlf*, *Mri*, and *Atm*, *Setd2* is not essential for C-NHEJ during V(D)J recombination (Bredemeyer et al., 2006; Zha et al., 2011; Hung et al., 2018). The non-essentiality of *Setd2*/H3K36me3 for end-joining was further intimated by the inability of dual loss of *Setd2*/H3K36me3 and *p53* to generate translocations leading to the development of proB-cell lymphomas (Figures S9A and S9B), unlike loss of core C-NHEJ factors in a *p53*-null background (Difilippantonio et al., 2000; Gao et al., 2000; Frank et al., 2000).

Despite not being required for end-joining, ATMi-treated *Setd2*$^{-/-}$ v-Abl cells exhibited significantly increased mis-repaired recombination products that corresponded to either repaired SJs but unrepaired CEs (SJ + CE) (Figures 5A, 5D(i-ii), and S8B) or the formation of hybrid joins (Figures 5A, 5D(i), and S8B), products consistent with the observed loss of GFP signal. The enhanced formation of HJs with loss of Atm kinase activity and *Setd2* was further corroborated by the increased detection of aberrant HJ products of the pMG-INV substrate in ATMi-treated *Setd2*$^{-/-}$ cells (Figure 5E). Although we could detect evidence of HJ formation by PCR of the recombination substrate in *Setd2*$^{-/-}$ lines without ATMi (Figure 5E), these products were below detection by Southern blotting (Figures 5D(i) and S8B), but consistent with the modest decrease in GFP signal with STI treatment alone (Figures 5B and 5C). Furthermore, we could detect HJ formation not only from the endogenous κ light chain locus of v-Abl *Setd2* knockout cells but also in *Setd2Δ/Δ* splenocytes (Figure 5F). Together, these data indicate a novel role for *Setd2*/H3K36me3, especially in combination with Atm kinase activity, in the repair phase of V(D)J recombination to ensure proper joining.

Loss of *Setd2*/H3K36me3 Reduces Overall B Cell Repertoire

Even without loss of Atm kinase activity, however, there was abundant evidence of aberrant and abnormal rearrangement of the endogenous Igh locus in primary *Setd2Δ/Δ* proB cells (Figures 4F and S5E). We sequenced a similarly sized recombination product, present in both control and *Setd2Δ/Δ* proB cells, for three different heavy chain Variable gene families joined to the J_H4 fragment and found additional abnormalities (Figure 6A). Loss of *Setd2*/H3K36me3 not only reduced the overall number of unique productive Igh rearrangements (assessed by the number of unique hypervariable complementarity defining region-3 [CDR3]) but also resulted in shortening of CDR3 length and reductions in N-nucleotide additions (Figures 6A and 6B) (Bolotin et al., 2017). Similarly, when we looked at RNA-based transcripts of productive rearrangements of the Igh locus in proB cells using the hypervariable region calling algorithm TRUST (Li et al., 2017; Hu et al., 2018, 2019), *Setd2Δ/Δ* proB cells exhibited significant decreases in detectable unique CDR3 sequences and an overall decrease in overall B cell repertoire diversity (Figures 6C and 6D). Furthermore, global variable and joining gene usage was reduced (Figure 6E) in proB cells from *Setd2Δ/Δ* mice and coincided with evidence of increased clonality in variable gene usage, which did not appear to be dependent on the proximity to the Diversity and Joining gene segment regions on the Igh locus (Figure 6F). These observations indicate that, in addition to its role with Atm during end-joining to ensure appropriate repair, *Setd2*/H3K36me3 is also involved in other mechanisms that prevent mis-processing and mis-repair of broken DNA ends to ensure the fidelity of V(D)J recombination and is critical in maintaining a normal immune repertoire.

Setd2/H3K36me3 Prevents Post-mitotic Neuronal Apoptosis and Perinatal Lethality

As *Setd2*/H3K36me3 seemed to be important for V(D)J recombination, we next wondered if it could play a role in Rag-independent C-NHEJ repair. To first test this, we assessed the sensitivity of asynchronous WT and *Setd2*$^{-/-}$ v-Abl cells to ionizing radiation and found that *Setd2*$^{-/-}$ v-Abl lines were more sensitive to DSBs induced by ionizing radiation (Figure 7A(i)). This increased sensitivity to ionizing radiation of

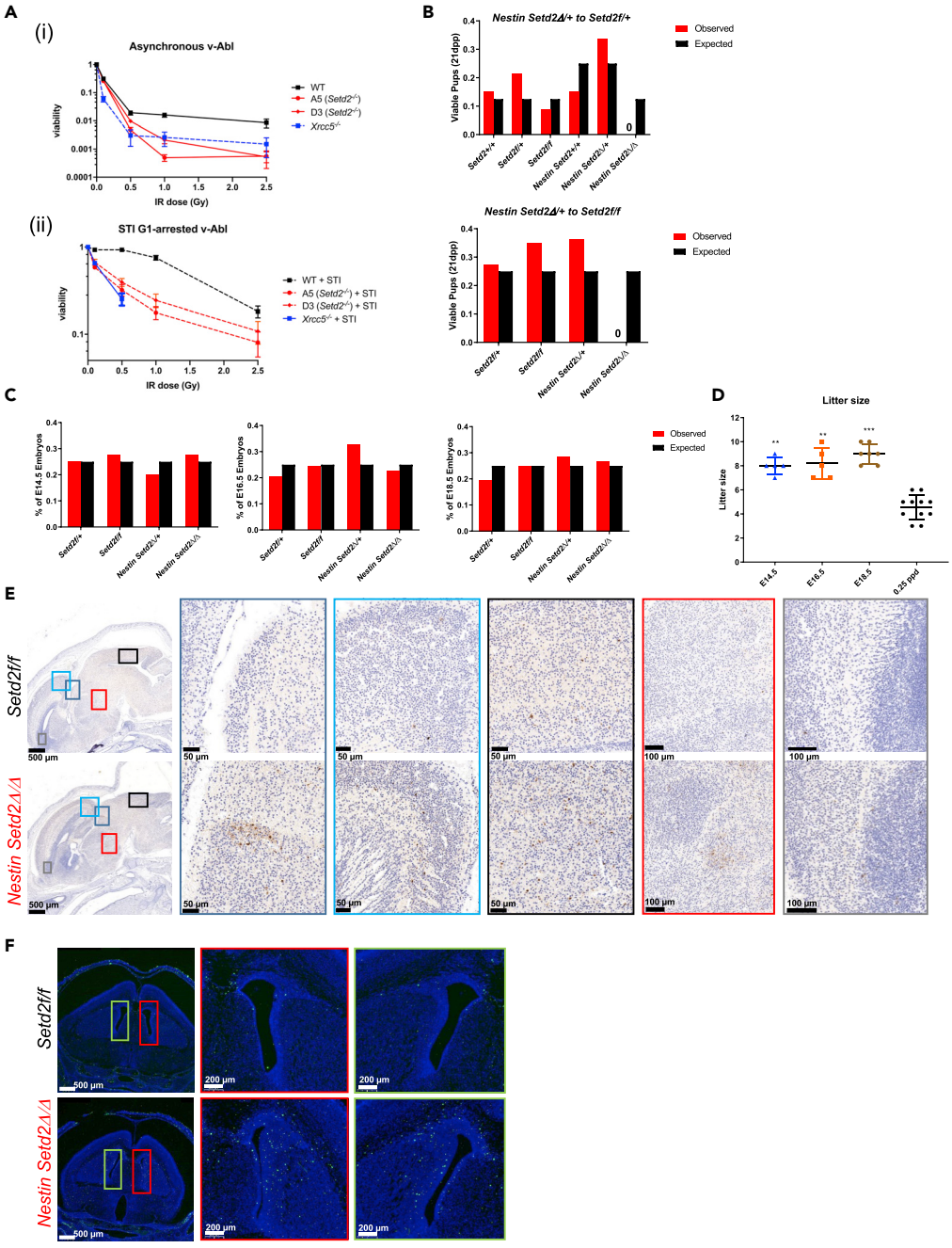

Figure 7. Post-mitotic Neuronal Apoptosis and Perinatal Lethality with Loss of *Setd2*/H3K36me3

(A) (i) Asynchronous and (ii) STI-571 G1-arrested WT, *Xrcc5*, and two different *Setd2*$^{-/-}$ v-Abl cells subjected to different doses of ionizing radiation and serially diluted five times in triplicate to assess survival. Values plotted as a mean of each dose as a percent of non-irradiated controls; bars represent standard deviation. Data are representative for three different independent treatment experiments. Viability was assessed at 72 h. No viable cells were detected beyond the 0.5 Gy dose for G1-arrested *Xrcc5* v-Abl clones.

(B) Expected and observed genotype distributions of matings between *Nestin-cre Setd2Δ/+* mice to *Setd2f/+* mice (n = 15 litters) and *Nestin-cre Setd2Δ/+* mice to *Setd2f/f* mice (n = 16 litters) 21 days post-partum (dpp).

(C) Embryo genotypes at different embryonic stages (n = 5 litters for each stage).

(D) Litter sizes of E14.5, E16.5, E18.5, and 0.25 dpp from *Nestin-cre Setd2Δ/+* mice to *Setd2f/f* breedings. Significance to 0.25 dpp was measured (n = 5 litters for each stage except 0.25 dpp, n = 11).

Figure 7. *Continued*

(E) Cleaved caspase 3 immunohistochemistry of E18.5 embryos. Sagittal sections show staining of regions of the diencephalic, telencephalic, and mesencephalic regions with magnifications indicated by corresponding colored boxes.
(F) TUNEL assay of 2-h post-partum control and *Nestin-cre Setd2Δ/Δ* pups. Coronal sections of the lateral ventricle with magnifications indicated by corresponding red and green boxes.
**p < 0.01 ***p < 0.001, error bars represent SD. See also Figures S10 and S11.

Setd2-deficient cells, at levels even greater than that of core NHEJ factors *Xrcc5* (*Ku80*) and *Lig4* (Figure 7A(i) and Figure S10A), could be in part due to previously described roles in HR-mediated DSB repair ascribed to *Setd2*/H3K36me3 (Li et al., 2013; Pfister et al., 2014; Aymard et al., 2014). To exclude the effects that may be driven by cells that may be cycling, we chose to study the sensitivity of G1-arrested v-Abl cells by inhibition with STI-571 or the Cdk4/6 inhibitor PD0332991 for 48 h before exposure to ionizing radiation. In both cell-cycle-arresting conditions, G1-arrested *Setd2*$^{-/-}$ v-Abl cells exhibited increased sensitivity cells to DSBs induced by ionizing radiation compared with WT controls (Figures 7A(ii), S10B, and S10C). Together, these data suggest that *Setd2*/H3K36me3 is important in the DSB repair in the G1 phase of cell cycle.

In addition to lymphogenesis, core C-NHEJ factors are critical for enforcing normal neurogenesis, where differentiating post-mitotic neurons migrating out of the ventricular zone do not have HR available for repair of DNA DSBs and instead rely on C-NHEJ (Frappart and McKinnon, 2008). Given our findings for a role for *Setd2*/H3K36me3 in the repair phase of V(D)J recombination, we tested its potential functions in neurogenesis. Consistent with the defective CNS development and embryonic lethality observed in knockout mouse models of core C-NHEJ factors (Gao et al., 1998; Frank et al., 2000; Gu et al., 2000), we observed post-mitotic neuronal apoptosis and perinatal lethality in mice with homozygous deletion of *Setd2* in neural progenitor-restricted *Nestin-cre*-expressing mice, where deletion has been demonstrated to occur before post-mitotic neurogenesis (Liang et al., 2012). The severity of this phenotype is demonstrated by the complete absence of *Nestin-cre Setd2Δ/Δ* pups at 21 days post-partum (dpp) (Figures 7B and 7C) with perinatal lethality by 0.25 dpp (Figure 7D). Histopathological analysis of embryos revealed evidence of apoptosis of post-mitotic neurons as early as E14.5 (Figures S11A and S11B), as well as more widespread apoptosis in the developing brain in E18.5 embryos and in 2-h post-partum pups (Figures 7E, 7F, S11C, and S11D) suggesting a role for *Setd2*/H3K36me3 in embryonic neurogenesis that is reminiscent of deficiency for C-NHEJ factors.

DISCUSSION

The preservation of a genome is predicated on proper repair of DNA DSB and a balance between HR, which is a highly accurate and also slower form of repair that is restricted to the availability of a sister chromatid strand, and NHEJ, which is highly efficient but intrinsically error prone (Takata et al., 1998). Although there have been some studies highlighting the importance of chromatin accessibility, nucleosome positioning, DNA looping, and recognition of histone modifications (e.g., H3K4me3 by RAG2) (Shimazaki and Lieber, 2014; Johnson et al., 2010; Bettridge et al., 2017; Matthews et al., 2007; Matheson and Corcoran, 2012) in the regulation of the V(D)J recombination process and phosphorylation of γH2AX in repair (Yin et al., 2009; Celeste et al., 2003), little has been described in terms of the impact of other chromatin modifications, especially in the end-joining phase of the V(D)J recombination reaction.

Here, we discovered a strong dependency of normal hematopoiesis and, in particular, lymphogenesis on *Setd2*/H3K36me3 phenotypes consistent with previously published reports of three distinctly engineered knockout mouse models (Zhou et al., 2018; Zhang et al., 2018; Ji et al., 2019). Early loss of *Setd2*/H3K36me3 leads to severely impaired B and T cell development that could be partially rescued, in the case of B lymphogenesis, with the expression of a fully rearranged Igh locus, pointing to a role for *Setd2*/H3K36me3 in V(D)J recombination. This role of *Setd2* in V(D)J recombination is further corroborated by the partial rescue of T lymphopoiesis with the over-expression of a rearranged TCR in *Lck*-cre *Setd2Δ/Δ* mice (Ji, et al., 2019). Ji et al. also report decreased Rag1 occupancy across the Igh locus in B220^{+}Cd19^{+} cells from *Cd19*cre *Setd2Δ/Δ* mice (Ji et al., 2019), including at variable region family genes. In sorted proB cells (B220^{+}Cd43^{+}IgM^{-}) where we induced loss of *Setd2*/H3K36me3 early in hematopoiesis, however, we could not detect a significant effect on the recruitment of Rag1 to the critical regulatory region near where the Eμ enhancer resides and where Rag1 has previously been shown to bind *in vivo* at the proB cell stage of development (Ji et al., 2010). The observed Rag1 occupancy differences observed by Ji et al., (2019) in populations of lymphoid cells are likely impacted by their inclusion of

more mature B cell populations ($B220^{+}Cd19^{+}$ includes $Cd43^{+}$ late proB and more mature Cd43-preB cells) that are depleted in *Setd2Δ/Δ* mice, as well as by incomplete and leaky deletion of *Setd2* via the use *cre*-expressing mouse lines (*Cd19cre*) that delete after the proB cell developmental stage of interest (Rickert et al., 1997; Hobeika et al., 2006; Kraus et al., 2004; Siegemund et al., 2015).

We wanted to understand the nature of the defect in repair with early loss of *Setd2* in proB cells, especially with respect to end-ligation, as we could not detect significant differences in the initiation phase of V(D)J recombination and as we could detect recombination of the Igh locus, albeit abnormal recombination. We therefore turned to an inducible system to measure the repair defect and uncovered new roles for *Setd2*/H3K36me3 in the fidelity of the V(D)J recombination reaction, especially in combination with ATM kinase activity. We determined that *Setd2*/H3K36me3 is not absolutely required for end-ligation by the lack of detectable unrepaired CEs and SEs of an ectopically integrated recombination substrate, pMG-INV. This non-essentiality for repair is consistent with our ability to detect recombination products in proB cells of *Setd2Δ/Δ* mice, albeit abnormal ones, and the lack of proB lymphomas as a consequence of translocation events in dual *Setd2Δ/Δ p53Δ/Δ* mice. It is noteworthy that unlike dual loss of ATM and XLF, loss of *Setd2*/H3K36me3 and Atm kinase activity did not result in complete abolishment of proper end-joining, but did lead to increased abnormal joining (e.g., SJ + CE joins and HJs), suggesting that *Setd2*/H3K36me3's role in end-ligation is functionally distinct from C-NHEJ *XRCC4* paralogs *XLF* and *PAXX* (Lescale et al., 2016; Kumar et al., 2016). Although we could detect robust and efficient conversion of fully and properly recombined SJ + CJ products of the pMG-INV recombination substrate in induced *Setd2*-deficient v-Abl cells, we could also detect, with combined loss of Atm kinase activity, an aberrant SJ + CE recombination product. This raises the possibility of a CE-specific hairpin opening/repair defect, which would certainly require further study as CEs are thought be efficiently processed and repaired at a much higher rate than SEs and CE-only defects have not previously been reported (Ramsden and Gellert, 1995; Schlissel et al., 1993; Roth, et al., 1992; Canela et al., 2016; Meek et al., 2016).

Paradoxically, whereas the end-ligation defect of *Setd2*/H3K36me3 loss, as determined by the assessment of a recombination substrate in transformed v-Abl cells, may appear subtle, in mice, its loss severely arrests normal B/T lymphocyte development, similar to what is observed in mice with loss of C-NHEJ factors (Alt et al., 2013; Kumar et al., 2014) and in contrast to loss of factors involved in end-ligation, such as Atm, Xlf, Paxx, or Mri individually (Bredemeyer et al., 2006; Kumar et al., 2016; Hung et al., 2018; Li et al., 2008; Lescale et al., 2016; Zha et al., 2011). This difference suggests that there are other determinants that contribute to the severe block in B (and T) lymphoid development in *Setd2* knockout mice. For example, certain factors present at the Igh locus in proB cells may not be fully recapitulated in the assessment of rearrangement of an ectopic recombination substrate in transformed v-Abl cells, potentially affecting both the efficiency and accuracy of repair.

Likewise, it is also possible that there are other roles of *ATM*, or *ATM* targets, and *SETD2* in end-joining that are not directly related and are mediated by distinct processes that, when combined, exacerbate mis-repair overall. Specifically, the loss of *Setd2*/H3K36me3 could influence the recruitment of factors associated with NHEJ in DNA DSB that recognize H3K36me3 (e.g., PHRF1 and PHF1) that could impact end-joining efficiency (Chang et al., 2015; Hong et al., 2008; Musselman et al., 2012), rather than playing a direct role in the stabilization of broken chromosomal ends, a function that has been ascribed to ATM (Bredemeyer et al., 2006). Additionally, we did not find any overt gene expression differences in alternative-NHEJ (A-NHEJ) factors and were not able to detect higher rates of deletions or translocations thought to accompany some forms of this A-NHEJ (Corneo et al., 2007) in either our CDR3 repertoire analysis, products of recombination of the recombination substrate in v-Abl cells, or in mice with dual loss of *Setd2* and *p53*. These correlative lines of evidence however, do not fully preclude the possibility of rare forms of A-NHEJ contributing to the observed phenotype, warranting further investigation.

When we examined the abnormal recombination in proB cells of *Setd2Δ/Δ* mice more closely, we additionally noted significant loss of B cell repertoire and reduction of variable gene usage, characterized by less diversity in re-arranged, productive CDR3 sequences, as well as other abnormalities. Shortening of CDR3 length, without concomitant reduction of immune repertoire, has been previously connected to end-ligation factor, *XLF* (IJspeert et al., 2016). In addition, shortening of CDR3 sequences of Ig heavy chain rearrangements has previously been observed in Pol X family knockouts (pol λ, μ), which with terminal deoxynucleotidyl transferase participates in nucleotide end-processing of heavy chain junctions during V(D)J

recombination (Bertocci et al., 2006). Thus, it is possible that *Setd2*/H3K36me3 may play additional roles in the end-processing of junctions, in addition to preventing the mis-repair in end-ligation we observed.

We also found that loss of *Setd2*/H3K36me3 increases sensitivity of cells to DSBs induced by ionizing radiation in both asynchronous and G1-arrested v-Abl cells, suggesting that *Setd2*/H3K36me3 may play a role in DSB repair activities in cells where HR would not be available, due to the lack of a sister chromatid. This result seemed to be supported by our discovery that neural-specific deletion of *Setd2*/H3K36me3 resulted in post-mitotic neuronal apoptosis. Although it is possible that other factors may be contributing to the neurogenesis defect, the temporal and spatial localization of apoptotic neuronal cells are highly suggestive of a role for *Setd2*/H3K36me3 in post-mitotic neurogenesis. The perinatal lethality we observed in *Nestin-cre Setd2Δ/Δ* mice is in stark contrast to *Nestin-cre*-driven conditional loss of core C-NHEJ factors, *Xrcc4* or *Lig4*, where mice survive to adulthood (Frappart et al., 2009; Yan et al., 2006). Instead, it parallels the severity of the developmental arrest we observed in lymphogenesis, despite *Setd2*/H3K36me3 not being essential for C-NHEJ repair.

Previous studies have indicated a role for H3K36me3 in not only the recruitment of components on DNA damage repair in both MMR (MSH2/6) (Li et al., 2013) and HR (CtIP) (Pfister et al., 2014; Aymard et al., 2014) but also a role in a myriad of other cellular processes (Wagner and Carpenter, 2012). Although we have not exhaustively ruled out every potential role of *Setd2*/H3K36me3 in DSB repair, transcription, and splicing, we have attempted to study the role of *Setd2*/H3K36me3 in two systems that utilize NHEJ-mediated DSB repair by taking advantage of the non-redundancy of *Setd2* in two independent mammalian developmental processes. Given the high frequency of *SETD2* mutations in B and T cell lymphomas (Parker et al., 2016; Zhang et al., 2012; McKinney et al., 2017; Moffitt et al., 2017), primary human immunodeficiency (Ji et al., 2019), and neurological/developmental disorders (e.g., autism, intellectual disability, high-grade pediatric glioma) (Fontebasso et al., 2013; D'Gama et al., 2015; Tlemsani et al., 2016; Lelieveld et al., 2016), our findings demonstrating a role of *Setd2*/H3K36me3 in normal lymphogenesis and neurogenesis are especially noteworthy.

Limitations of Studies

Limitations of our studies include our inability to assess localization of critical NHEJ factors (e.g., Rag2, Ku70, Ku80, Xrcc4, Lig4, and others) due to the lack of readily available antibodies to perform ChIP of these proteins. In addition, although the use of v-Abl-transformed late-proB cell lines with an ectopically expressed recombination substrate can determine the essentiality of factors for end-joining in NHEJ, the use of such a system fails to recapitulate the factors or genomic structure present at the endogenous immunoglobulin loci, which may also influence the V(D)J recombination process during early lymphocyte development. Thus, it is possible that the severity of the block in normal lymphocyte development observed *in vivo* could be influenced by factors and mechanisms beyond the role of *Setd2*/H3K36me3 in end-joining during the repair phase of V(D)J recombination. Also, we were unable to assess if there was a non-enzymatic role for the Setd2 protein itself in any of the NHEJ processes in lymphocyte development, as expression of a full-length Setd2 (~2,500 amino acids, ~8-kb nucleotide coding sequence) in primary murine cells was unable to be achieved (by us and also not reported by other groups with genetically engineered Setd2 knockout mouse models, including but limited to Zhou et al., 2018; Zhang et al., 2018; Ji et al., 2019). We also did not fully and exhaustively investigate the role of A-NHEJ factors or the potential contribution of other roles that Setd2 and H3K36me3 play in normal cellular processes in both V(D)J recombination or post-mitotic neurogenesis settings.

METHODS

All methods can be found in the accompanying Transparent Methods supplemental file.

DATA AND CODE AVAILABILITY

RNA-seq, ATAC-seq, ChIP-seq, TRUST, and MIXCR data generated and analyzed during the current study have been deposited into the National Center for Biotechnology Information (NCBI) Gene Expression Omnibus (GEO). The accession numbers for the RNA-seq, ATAC-seq, ChIP-seq, TRUST, and MIXCR data reported in this paper are GSE130904, GSE131588, GSE131608. These are unified under SuperSeries GSE131690.

SUPPLEMENTAL INFORMATION

Supplemental Information can be found online at https://doi.org/10.1016/j.isci.2020.100941.

ACKNOWLEDGMENTS

The authors thank the Armstrong Laboratory for helpful feedback and fruitful scientific suggestions. We thank Dr. Fred W. Alt for experimental discussions, feedback, and critical review. We would also like to thank Charlie Hatton for help with GEO submissions. We thank the flow cytometry cores at Memorial Sloan-Kettering Cancer Center and Dana Farber Cancer Institute (Hematologic Neoplasia Core) for assistance in cell sorting, MGH Center for Computation and Integrative Biology DNA core for complete amplicon NGS sequencing, and the Dana-Farber Harvard Medical School rodent pathology core and Servicebio Inc. for support in histological analyses for these studies. This work was supported by National Institutes of Health, National Cancer Institute grants R01 CA176745 and 5P01 CA066996(SAA). S.H.C. is a Damon Runyon-Sohn Pediatric Fellow supported by the Damon Runyon Cancer Research Foundation (DRSG-5-13). V.K. is supported by an NCI 5F30CA189740-05. J.Z. was funded by the Chinese Scholarship Council. Funding. The Nussenzweig Laboratory is supported by the Intramural Research Program of the National Institutes of Health, the National Cancer Institute, Center for Cancer Research, and a Alex's Lemonade Stand Foundation Award. The Sleckman laboratory is supported by NIH grants R01s AI047829 and AI074953.

AUTHOR CONTRIBUTIONS

S.H.C. and S.A.A. designed experiments and wrote the paper. S.H.C., J.R.C., C.N.M., J.C.M., Y.X., and B.-R.C. performed experiments. J.Z. performed MiXCR and TRUST analyses, and R.P.K. performed bioinformatics analyses. V.K., E.C., P.J.H., Z.F., X.S.L., J.C., A.N., and B.P.S. provided experimental support and reagents for these studies as well as critical review of this paper.

DECLARATION OF INTERESTS

S.A.A. has been a consultant and/or shareholder for Epizyme Inc, Imago Biosciences, Cyteir Therapeutics, C4 Therapeutics, Syros Pharmaceuticals, OxStem Oncology, Accent Therapeutics, and Mana Therapeutics. S.A.A. has received research support from Janssen, Novartis, and AstraZeneca. S.H.C. is currently an employee at Beam Therapeutics. The authors have no additional financial interests.

Received: October 7, 2019
Revised: January 25, 2020
Accepted: February 21, 2020
Published: March 27, 2020

REFERENCES

Abramowski, V., Etienne, O., Elsaid, R., Yang, J., Berland, A., Kermasson, L., Roch, B., Musilli, S., Moussu, J.P., Lipson-Ruffert, K., et al. (2018). PAXX and Xlf interplay revealed by impaired CNS development and immunodeficiency of double KO mice. Cell Death Differ. *25*, 444–452.

Alt, F.W., Zhang, Y., Meng, F.L., Guo, C., and Schwer, B. (2013). Mechanisms of programmed DNA lesions and genomic instability in the immune system. Cell *52*, 417–429.

Aymard, F., Bulger, B., Schmid, C.K., Guillou, E., Caron, P., Briois, S., Iacovoni, J.S., Daburon, V., Miller, K.M., Jackson, S.P., and Legube, G. (2014). Transcriptionally active chromatin recruits homologous recombination at DNA double-strand breaks. Nat. Struct. Mol. Biol. *21*, 366–374.

Bassing, C.H., Swat W, W., and Alt, F.W. (2002). The mechanism and regulation of chromosomal V(D)J recombination. Cell *109*, S45–S55.

Bertocci, B., De Smet, A., Weill, J.C., and Reynaud, C.A. (2006). Nonoverlapping functions of DNA polymerases mu, lambda, and terminal deoxynucleotidyltransferase during immunoglobulin V(D)J recombination in vivo. Immunity *25*, 31–41.

Bettridge, J., Na, C.H., Pandey, A., and Desiderio, S. (2017). H3K4me3 induces allosteric conformational changes in the DNA-binding and catalytic regions of the V(D)J recombinase. Proc. Natl. Acad. Sci. U S A *114*, 1904–1909.

Bolotin, D.A., Poslavsky, S., Davydov, A.N., Frenkel, F.E., Fanchi, L., Zolotareva, O.I., Hemmers, S., Putintseva, E.V., Obraztsova, A.S., Shugay, M., et al. (2017). Antigen receptor repertoire profiling from RNA-seq data. Nat. Biotechnol. *35*, 908–911.

Bredemeyer, A.L., Sharma, G.G., Huang, C.Y., Helmink, B.A., Walker, L.M., Khor, K.C., Nuskey, B., Sullivan, K.E., Pandita, T.K., Bassing, C.H., and Sleckman, B.P. (2006). ATM stabilizes DNA double-strand-break complexes during V(D)J recombination. Nature *442*, 466–470.

Canela, A., Sridharan, S., Sciascia, N., Tubbs, A., Meltzer, P., Sleckman, B.P., and Nussenzweig, A. (2016). DNA breaks and end resection measured genome-wide by end sequencing. Mol. Cell *63*, 1–14.

Celeste, A., Difilippantonio, S., Difilippantonio, M.J., Fernandez-Capetillo, O., Pilch, D.R., Sedelnikova, O.A., Eckhaus, M., Ried, T., Bonner, W.M., and Nussenzweig, A. (2003). H2AX haploinsufficiency modifies genomic stability and tumor susceptibility. Cell *114*, 371–383.

Chakraborty, T., Perlot, T., Subrahmanyam, R., Jani, A., Goff, P.H., Zhang, Y., Ivanova, I., Alt, F.W., and Sen, R. (2009). A 220-nucleotide deletion of the intronic enhancer reveals an epigenetic hierarchy in immunoglobulin heavy chain locus activation. J. Exp. Med. *206*, 1019–1027.

Chang, C.F., Chu, P.C., Wu, P.Y., Yu, M.Y., Lee, J.Y., Tsai, M.D., and Chang, M.S. (2015). PHRF1 promotes genome integrity by modulating non-homologous end-joining. Cell Death Dis. *6*, e1716.

Chowdhury, D., and Sen, R. (2001). Stepwise activation of the immunoglobulin mu heavy chain gene locus. EMBO J. *20*, 6394–6403.

Corneo, B., Wendland, R.L., Deriano, L., Cui, X., Klein, I.A., Wong, S.Y., Arnal, S., Holub, A.J., Weller, G.R., Pancake, B.A., et al. (2007). Rag mutations reveal robust alternative end joining. Nature *449*, 483–486.

D'Gama, A.M., Pochareddy, S., Li, M., Jamuar, S.S., Reiff, R.E., Lam, A.N., Sestan, N., and Walsh, C.A. (2015). Targeted DNA sequencing from autism spectrum disorder brains implicates multiple genetic mechanisms. Neuron *88*, 910–917.

Difilippantonio, M.J., Zhu, J., Chen, H.T., Meffre, E., Nussenzweig, M.C., Max, E.E., Ried, T., and Nussenzweig, A. (2000). DNA repair protein Ku80 suppresses chromosomal aberrations and malignant transformation. Nature *404*, 510–514.

Fnu, S., Williamson, E.A., De Haro, L.P., Brenneman, M., Wray, J., Shaheen, M., Radhakrishnan, K., Lee, S.H., Nickoloff, J.A., and Hromas, R. (2011). Methylation of histone H3 lysine 36 enhances DNA repair by nonhomologous end-joining. Proc. Natl. Acad. Sci. U S A *108*, 540–545.

Fontebasso, A.M., Schwartzentruber, J., Khuong-Quang, D.A., Liu, X.Y., Sturm, D., Korshunov, A., Jones, D.T., Witt, H., Kool, M., Albrecht, S., et al. (2013). Mutations in SETD2 and genes affecting histone H3K36 methylation target hemispheric high-grade gliomas. Acta Neuropathol. *125*, 659–669.

Frank, K.M., Sharpless, N.E., Gao, Y., Sekiguchi, J.M., Ferguson, D.O., Zhu, C., Manis, J.P., Horner, J., DePinho, R.A., and Alt, F.W. (2000). DNA ligase IV deficiency in mice leads to defective neurogenesis and embryonic lethality via the p53 pathway. Mol. Cell *5*, 993–1002.

Frappart, P.O., and McKinnon, P.J. (2008). Mouse models of DNA double-strand break repair and neurological disease. DNA Repair (Amst) *7*, 1051–1060.

Frappart, P.O., Lee, Y., Russell, H.R., Chalhoub, N., Wang, Y.D., Orii, K.E., Zhao, J., Kondo, N., Baker, S.J., and McKinnon, P.J. (2009). Recurrent genomic alterations characterize medulloblastoma arising from DNA double-strand break repair deficiency. Proc. Natl. Acad. Sci. U S A *106*, 1880–1885.

Gao, Y., Sun, Y., Frank, K.M., Dikkes, P., Fujiwara, Y., Seidl, K.J., Sekiguchi, J.M., Rathbun, G.A., Swat, W., Wang, J., et al. (1998). A critical role for DNA end-joining proteins in both lymphogenesis and neurogenesis. Cell *95*, 891–902.

Gao, Y., Ferguson, D.O., Xie, W., Manis, J.P., Sekiguchi, J., Frank, K.M., Chaudhuri, J., Horner, J., DePinho, R.A., and Alt, F.W. (2000). Interplay of p53 and DNA-repair protein XRCC4 in tumorigenesis, genomic stability and development. Nature *404*, 897–900.

Gu, Y., Sekiguchi, J., Gao, Y., Dikkes, P., Frank, K., Ferguson, D., Hasty, P., Chun, J., and Alt FW, F.W. (2000). Defective embryonic neurogenesis in Ku-deficient but not DNA-dependent protein kinase catalytic subunit-deficient mice. Proc. Natl. Acad. Sci. U S A *97*, 2668–2673.

Hobeika, E., Thiemann, S., Storch, B., Jumaa, H., Nielsen, P.J., Pelanda, R., and Reth, M. (2006). Testing gene function early in the B cell lineage in mb1-cre mice. Proc. Natl. Acad. Sci. U S A *103*, 13789–13794.

Hong, Z., Jiang, J., Lan, L., Nakajima, S., Kanno, S., Koseki, H., and Yasui, A. (2008). A polycomb group protein, PHF1, is involved in the response to DNA double-strand breaks in human cell. Nucleic Acids Res. *36*, 2939–2947.

Hu, M., Sun, X.J., Zhang, Y.L., Kuang, Y., Hu, C.Q., Wu, W.L., Shen, S.H., Du, T.T., Li, H., He, F., et al. (2010). Histone H3 lysine 36 methyltransferase Hypb/Setd2 is required for embryonic vascular remodeling. Proc. Natl. Acad. Sci. U S A *107*, 2956–2961.

Hu, X., Zhang, J., Liu, J.S., Li, B., and Liu, X.S. (2018). Evaluation of immune repertoire inference methods from RNA-seq data. Nat. Biotechnol. *36*, 1034.

Hu, X., Zhang, J., Wang, J., Fu, J., Li, T., Zheng, X., Wang, B., Gu, S., Jiang, P., Fan, J., et al. (2019). Landscape of B cell immunity and related immune evasion in human cancers. Nat. Genet. *51*, 560–567.

Hung, P.J., Johnson, B., Chen, B.R., Byrum, A.K., Bredemeyer, A.L., Yewdell, W.T., Johnson, T.E., Lee, B.J., Deivasigamani, S., Hindi, I., et al. (2018). MRI is a DNA damage response adaptor during classical non-homologous end joining. Mol. Cell *71*, 332–342.

IJspeert, H., Rozmus, J., Schwarz, K., Warren, R.L., van Zessen, D., Holt, R.A., Pico-Knijnenburg, I., Simons, E., Jerchel, I., Wawer, A., et al. (2016). XLF deficiency results in reduced N-nucleotide addition during V(D)J recombination. Blood *128*, 650–659.

Jacobsen, E.A., Ananieva, O., Brown, M.L., and Chang, Y. (2006). Growth, differentiation, and malignant transformation of pre-B cells mediated by inducible activation of v-Abl oncogene. J. Immunol. *176*, 6831–6838.

Johnson, K., Chaumeil, J., and Skok, J.A. (2010). Epigenetic regulation of V(D)J recombination. Essays Biochem. *48*, 221–243.

Ji, Y., Resch, W., Corbett, E., Yamane, A., Casellas, R., and Schatz, D.G. (2010). The in vivo pattern of binding of RAG1 and RAG2 to antigen receptor loci. Cell *141*, 419–431.

Ji, Z., Sheng, Y., Miao, J., Li, X., Zhao, H., Wang, J., Cheng, C., Wang, X., Liu, K., Zhang, K., et al. (2019). The histone methyltransferase Setd2 is indispensable for V(D)J recombination. Nat. Commun. *10*, 3353.

Kraus, M., Alimzhanov, M.B., Rajewsky, N., and Rajewsky, K. (2004). Survival of resting mature B lymphocytes depends on BCR signaling via the Igalpha/beta heterodimer. Cell *117*, 787–800.

Kumar, V., Alt, F.W., and Frock, R.L. (2016). PAXX and XLF DNA repair factors are functionally redundant in joining DNA breaks in a G1-arrested progenitor B-cell line. Proc. Natl. Acad. Sci. U S A *113*, 10619–10624.

Kumar, V., Alt, F.W., and Oksenych, V. (2014). Functional overlaps between XLF and the ATM-dependent DNA double strand break response. DNA Repair (Amst). *16*, 11–22.

Lelieveld, S.H., Reijnders, M.R., Pfundt, R., Yntema, H.G., Kamsteeg, E.J., de Vries, P., de Vries, B.B., Willemsen, M.H., Kleefstra, T., Löhner, K., et al. (2016). Meta-analysis of 2,104 trios provides support for 10 new genes for intellectual disability. Nat. Neurosci. *19*, 1194–1196.

Lescale, C., Abramowski, V., Bedora-Faure, M., Murigneux, V., Vera, G., Roth DB, D.B., Revy, P., de Villartay, J.P., and Deriano, L. (2016). RAG2 and XLF/Cernunnos interplay reveals a novel role for the RAG complex in DNA repair. Nat. Commun. *7*, 10529.

Li, B., Li, T., Wang, B., Dou, R., Zhang, J., Liu, J.S., and Liu, X.S. (2017). Ultrasensitive detection of TCR hypervariable-region sequences in solid-tissue RNA–seq data. Nat. Genet. *49*, 482–483.

Li, F., Mao, G., Tong, D., Huang, J., Gu, L., Yang, W., and Li, G.M. (2013). The histone mark H3K36me3 regulates human DNA mismatch repair through its interaction with MutSα. Cell *153*, 590–600.

Li, G., Alt FW, F.W., Cheng, H.L., Brush, J.W., Goff, P.H., Murphy, M.M., Franco, S., Zhang, Y., and Zha, S. (2008). Lymphocyte-specific compensation for XLF/cernunnos end-joining functions in V(D)J recombination. Mol. Cell *31*, 631–640.

Liang, H., Hippenmeyer, S., and Ghashghaei, H.T. (2012). A Nestin-cre transgenic mouse is insufficient for recombination in early embryonic neural progenitors. Biol. Open *1*, 1200–1203.

Lu, C., Jain, S.U., Hoelper, D., Bechet, D., Molden, R.C., Ran, L., Murphy, D., Venneti, S., Hameed, M., Pawel, B.R., et al. (2016). Histone H3K36 mutations promote sarcomagenesis through altered histone methylation landscape. Science *352*, 844–849.

Mar, B.G., Chu, S.H., Kahn, J.D., Krivtsov, A.V., Koche, R., Castellano, C.A., Kotlier, J.L., Zon, R.L., McConkey, M.E., Chabon, J., et al. (2017). SETD2 alterations impair DNA damage recognition and lead to resistance to chemotherapy in leukemia. Blood *130*, 2631–2641.

Matheson, L.S., and Corcoran, A.E. (2012). Local and global epigenetic regulation of V(D)J recombination. Curr. Top. Microbiol. Immunol. *356*, 65–89.

Matthews, A.G., Kuo, A.J., Ramón-Maiques, S., Han, S., Champagne, K.S., Ivanov, D., Gallardo, M., Carney, D., Cheung, P., Ciccone, D.N., et al. (2007). RAG2 PHD finger couples histone H3 lysine 4 trimethylation with V(D)J recombination. Nature *450*, 1106–1110.

McKinney, M., Moffitt, A.B., Gaulard, P., Travert, M., De Leval, L., Nicolae, A., Raffeld, M., Jaffe, E.S., Pittaluga, S., Xi, L., et al. (2017). The genetic basis of hepatosplenic T-cell lymphoma. Cancer Discov. *7*, 369–379.

Meek, K., Xu, Y., Bailie, C., Kefei, Y., and Neal, J.A. (2016). The ATM kinase restrains joining of both VDJ signal and coding ends. J. Immunol. *197*, 3165–3174.

Moffitt, A.B., Ondrejka, S.L., McKinney, M., Rempel, R.E., Goodlad, J.R., Teh, C.H., Leppa, S.,

Mannisto, S., Kovanen, P.E., Tse, E., et al. (2017). Enteropathy-associated T cell lymphoma subtypes are characterized by loss of function of SETD2. J. Exp. Med. *214*, 1371–1386.

Musselman, C.A., Avvakumov, N., Watanabe, R., Abraham, C.G., Lalonde, M.E., Hong, Z., Allen, C., Roy, S., Nuñez, J.K., Nickoloff, J., et al. (2012). Molecular basis for H3K36me3 recognition by the Tudor domain of PHF1. Nat. Struct. Mol. Biol. *19*, 1266–1272.

Parker, H., Rose-Zerilli, M.J., Larrayoz, M., Clifford, R., Edelmann, J., Blakemore, S., Gibson, J., Wang, J., Ljungström, V., Wojdacz, T.K., et al. (2016). Genomic disruption of the histone methyltransferase SETD2 in chronic lymphocytic leukaemia. Leukemia *30*, 2179–2186.

Pfister, S.X., Ahrabi, S., Zalmas, L.P., Sarkar, S., Aymard, F., Bachrati, C.Z., Helleday, T., Legube, G., La Thangue, N.B., Porter, A.C., and Humphrey, T.C. (2014). SETD2-dependent histone H3K36 trimethylation is required for homologous recombination repair and genome stability. Cell Rep. *7*, 2006–2018.

Ramsden, D.A., and Gellert, M. (1995). Formation and resolution of double-strand break intermediates in V(D)J rearrangement. Genes Dev. *9*, 2409–2420.

Rickert, R.C., Roes, J., and Rajewsky, K. (1997). B lymphocyte-specific, Cre-mediated mutagenesis in mice. Nuclei Acids Res. *25*, 1317–1318.

Roth, D.B., Menetski, J.P., Nakajima, P.B., Bosma, M.J., and Gellert, M. (1992). V(D)J recombination: broken DNA molecules with covalently sealed (hairpin) coding ends in scid mouse thymocytes. Cell *70*, 983–991.

Schatz, F.G., and Swanson, P.G. (2001). V(D)J recombination: mechanisms of initiation. Annu. Rev. Genet. *45*, 167–202.

Schlissel, M., Constantinescu, A., Morrow, T., Baxter, M., and Peng, A. (1993). Double-strand signal sequence breaks in V(D)J recombination are blunt, 5′-phosphorylated, RAG-dependent, and cell cycle regulated. Genes Dev. *7*, 2520–2532.

Siegemund, S., Shepherd, J., Xiao, C., and Sauer, K. (2015). hCD2-iCre and Vav-iCre mediated gene recombination patterns in murine hematopoietic cells. PLoS One *10*, e0124661.

Shimazaki, N., and Lieber, M.R. (2014). Histone methylation and V(D)J recombination. Int. J. Hematol. *100*, 230–237.

Takata, M., Sasaki, M.S., Sonoda, E., Morrison, C., Hashimoto, M., Utsumi, H., Yamaguchi-Iwai, Y., Shinohara, A., and Takeda, S. (1998). Homologous recombination and non-homologous end-joining pathways of DNA double-strand break repair have overlapping roles in the maintenance of chromosomal integrity in vertebrate cells. EMBO J. *17*, 5497–5508.

Tlemsani, C., Luscan, A., Leulliot, N., Bieth, E., Afenjar, A., Baujat, G., Doco-Fenzy, M., Goldenberg, A., Lacombe, D., Lambert, L., et al. (2016). SETD2 and DNMT3A screen in the Sotos-like syndrome French cohort. J. Med. Genet. *53*, 743–751.

Wagner, E.J., and Carpenter, P.B. (2012). Understanding the language of Lys36 methylation at histone H3. Nat. Rev. Mol. Cell Biol. *23*, 115–126.

Yan, C.T., Kaushal, D., Murphy, M., Zhang, Y., Datta, A., Chen, C., Monroe, B., Mostoslavsky, G., Coakley, K., Gao, Y., et al. (2006). XRCC4 suppresses medulloblastomas with recurrent translocations in p53-deficient mice. Proc. Natl. Acad. Sci. U S A *103*, 7378–7383.

Yin, B., Savic, V., Juntilla, M.M., Bredemeyer, A.L., Yang-Iott, K.S., Helmink, B.A., Koretzky, G.A., Sleckman, B.P., and Bassing, C.H. (2009). Histone H2AX stabilizes broken DNA strands to suppress chromosome breaks and translocations during V(D)J recombination. J. Exp. Med. *206*, 2625–2639.

Zha, S., Guo, C., Boboila, C., Oksenych, V., Cheng, H.L., Zhang, Y., Wesemann, D.R., Yuen, G., Patel, H., Goff, P.H., et al. (2011). ATM damage response and XLF repair factor are functionally redundant in joining DNA breaks. Nature *469*, 250–254.

Zhang, J., Ding, L., Holmfeldt, L., Wu, G., Heatley, S.L., Payne-Turner, D., Easton, J., Chen, X., Wang, J., Rusch, M., et al. (2012). The genetic basis of early T-cell precursor acute lymphoblastic leukaemia. Nature *481*, 157–163.

Zhang, Y.L., Sun, J.W., Xie, Y.Y., Zhou, Y., Liu, P., Song, J.C., Xu, C.H., Wang, L., Liu, D., Xu, A.N., et al. (2018). Setd2 deficiency impairs hematopoietic stem cell self-renewal and causes malignant transformation. Cell Res. *28*, 476–790.

Zhou, Y., Yan, X., Feng, X., Bu, J., Dong, Y., Lin, P., Hayashi, Y., Huang, R., Olsson, A., Andreassen, P.R., et al. (2018). Setd2 regulates quiescence and differentiation of adult hematopoietic stem cells by restricting RNA polymerase II elongation. Hematologica *103*, 110–1123.

Zhu, X., He, F., Zeng, H., Ling, S., Chen, A., Wang, Y., Yan, X., Wei, W., Pang, Y., Cheng, H., et al. (2014). Identification of functional cooperative mutations of SETD2 in human acute leukemia. Nat. Genet. *46*, 287–293.

iScience, Volume *23*

Supplemental Information

Loss of H3K36 Methyltransferase SETD2 Impairs V(D)J Recombination during Lymphoid Development

S. Haihua Chu, Jonathan R. Chabon, Chloe N. Matovina, Janna C. Minehart, Bo-Ruei Chen, Jian Zhang, Vipul Kumar, Yijun Xiong, Elsa Callen, Putzer J. Hung, Zhaohui Feng, Richard P. Koche, X. Shirley Liu, Jayanta Chaudhuri, Andre Nussenzweig, Barry P. Sleckman, and Scott A. Armstrong

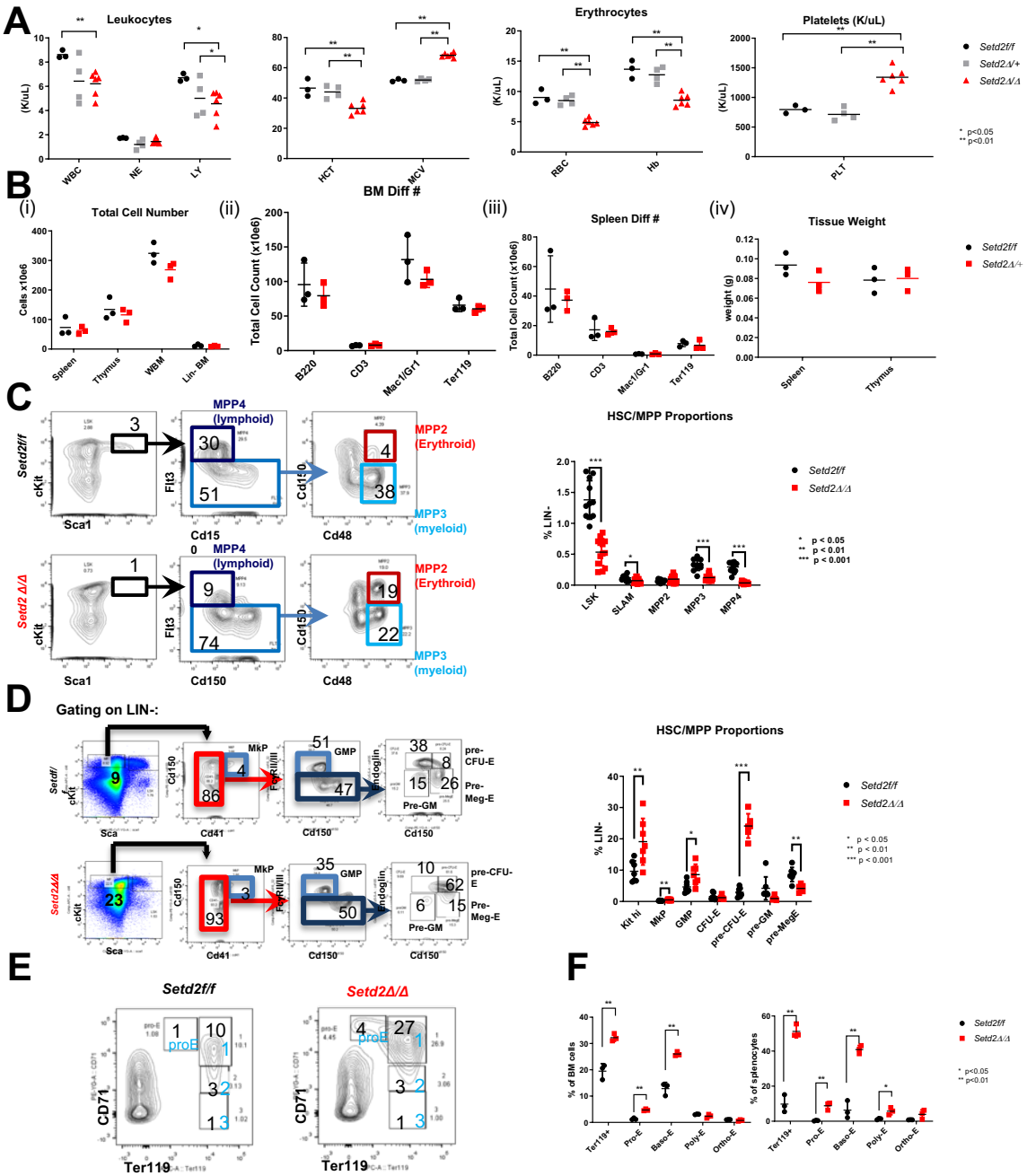

Figure S1. Loss of *Setd2*/H3K36me3 disrupts normal hematopoiesis, Related to Figure 1

(A) CBC and differentials from *Setd2Δ/Δ, Setd2Δ/+* and controls (*Setd2f/f*) (n≥3 for all groups) *, p<0.05 **, p<0.01 ***, p<0.001 **(B)** (i) total cellularity of spleen, thymus, whole bone marrow and lineage negative BM, total cellularity of cells positive for differentiated markers B220, Cd3, Mac1, Gr1, or Ter119 in (ii) bone marrow or (iii) spleen and (iv) spleen and thymus weights for heterozygous *Setd2* mice and controls (n= 3 for all groups). All values were non-significant. **(C)** Representative flow cytometry plot of HSC fractions, multipotent primed progenitors (MPP1-4) and percent composition of lineage negative cells of HSC stem cell and progenitor populations (n= 10 for all groups). **(D)** Representative flow cytometry plots for early myeloid and erythroid progenitor populations in bone marrow. MkP: Kit^{hi}Sca1^{-}Cd41^{+}Cd150^{+}, GMP: Kit^{hi}Sca1^{-}Cd41^{-}Cd150^{-}FcγRII/III^{+}, pre-GM: Kit^{hi}Sca1^{-}Cd41^{-}FcγRII/III^{-}Cd150^{-}Endoglin^{-}, pre-CFU-E: Kit^{hi}Sca1^{-}Cd41^{-}FcγRII/III^{-}Cd150^{+}Endoglin^{+}, pre-MegE: Kit^{hi}Sca1^{-}Cd41^{-}FcγRII/III^{-}Cd150^{+}Endoglin^{-} and proportion of HSC and erythroid progenitor populations of control and *Setd2Δ/Δ* (n = 7 for all groups). **(E)** Representative flow cytometry of erythroid progenitor populations. proE, 1-Basophilic erythroblasts (Baso-E), 2-late Baso-E and chromatophilic erythroblasts (Poly-E), and 3-orthochromatophilic erythroblasts (Ortho-E) in control and *Setd2Δ/Δ* bone marrow. **(F)** Percent composition of different erythroid progenitor populations in bone marrow and spleen of control and *Setd2Δ/Δ* mice (n = 3). *, p<0.05 **, p<0.01 ***, p<0.001, error bars represent SD.

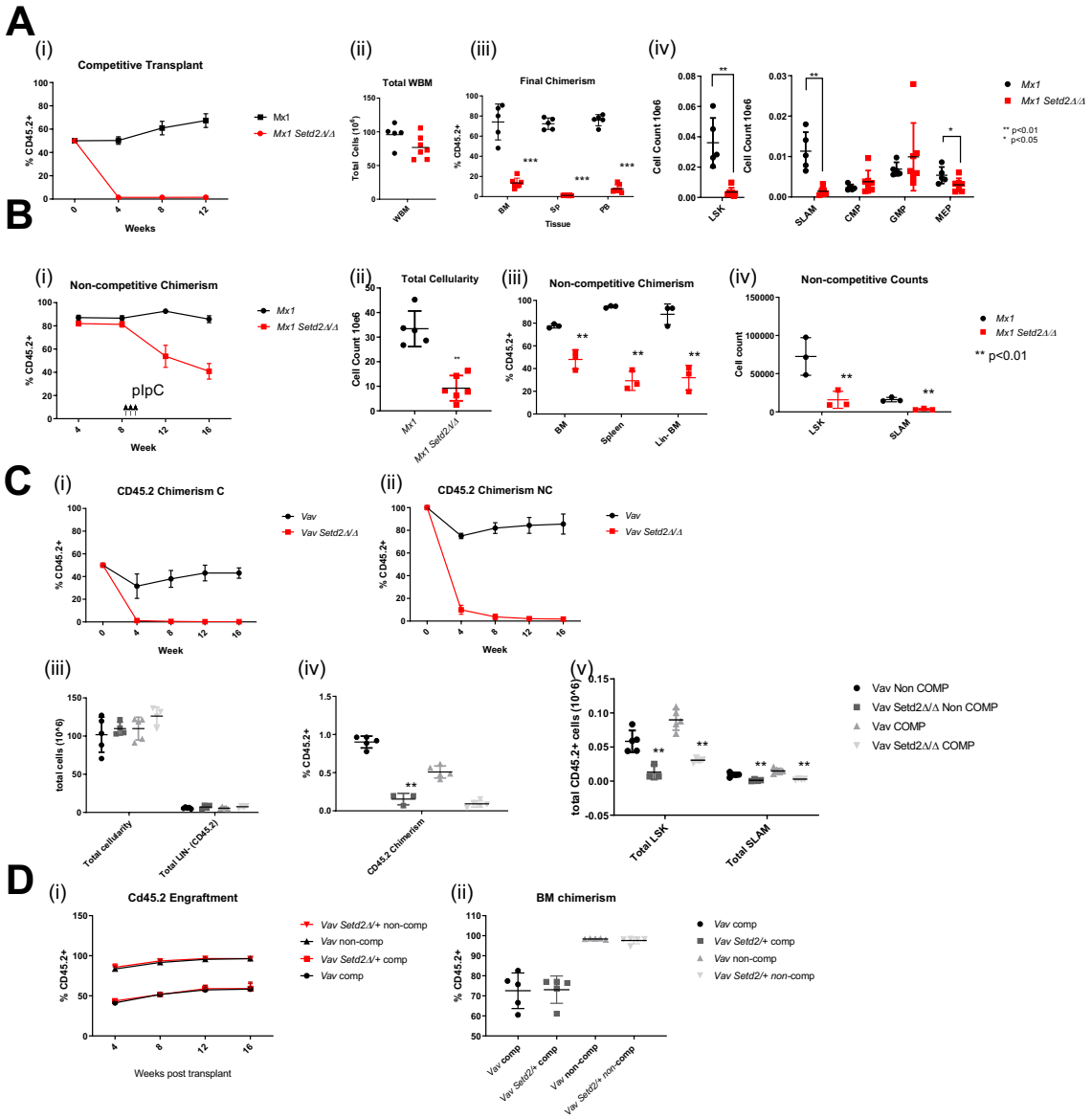

Figure S2. *Setd2Δ/Δ* HSCs are defective in competitive and non-competitive bone marrow (BM) reconstitution assays, Related to Figure 1

(A) (i) Peripheral blood engraftment, as measured by Cd45.2$^+$ of competitive reconstitution of lethally irradiated (9cGy) recipient mice with 1x10^6 WBM *Mx1 Setd2Δ/Δ* and control bone marrow with 1x10^6 WBM from syngeneic Cd45.1$^+$ mice after induction of Mx1-cre with polyI:polyC (pIpC). (ii) Total BM cellularity of mice 16 weeks after induction with pIpC (iii) percent Cd45.2 involvement in BM, spleen and peripheral blood, (iv) total cell counts of Cd45.2$^+$ donor HSC stem and progenitor populations. **(B)** Non-competitive reconstitution assay as conducted in (A) without 1x10^6 Cd45.1$^+$ wildtype competitor WBM cells. Arrows indicate when pIpC treatment was initiated. (ii-iv) graphs were generated from mice 28 days post pIpC induction as *Setd2Δ/Δ* mice were moribund due to complete BM failure. **(C)** Competitive and non-competitive reconstitution of lethally irradiated (9cGy) recipient mice with 1x10^6 WBM *Vav-cre Setd2Δ/Δ* and control BM with 1x10^6 WBM from syngeneic Cd45.1$^+$ mice. Overall peripheral blood Cd45.2 chimerism in (i) competitive and (ii) non-competitive reconstitution assays. (iii) total cellularity of Cd45.2$^+$ whole and lineage negative BM (iv) Cd45.2$^+$ chimerism (v) percentage and total numbers of Cd45.2$^+$ donor derived HSC of competitive and non-competitive transplants 16 weeks post-transplant **(D)** Competitive and non-competitive reconstitution of lethally irradiated recipient mice with 1x10^6 WBM *Vav-cre Setd2Δ/Δ* and *Vav-cre Setd2Δ/+* control BM with 1x10^6 WBM from syngeneic Cd45.1$^+$ mice. (i) Overall peripheral blood Cd45.2$^+$ chimerism and (ii) BM Cd45.2$^+$ chimerism in competitive and non-competitive reconstitution assays 16 weeks post-transplant. All data is representative of at least 3 independent transplant experiments. n = 5 for each transplant group. *, p<0.05 **, p<0.01 ***, p<0.001, error bars represent SD.

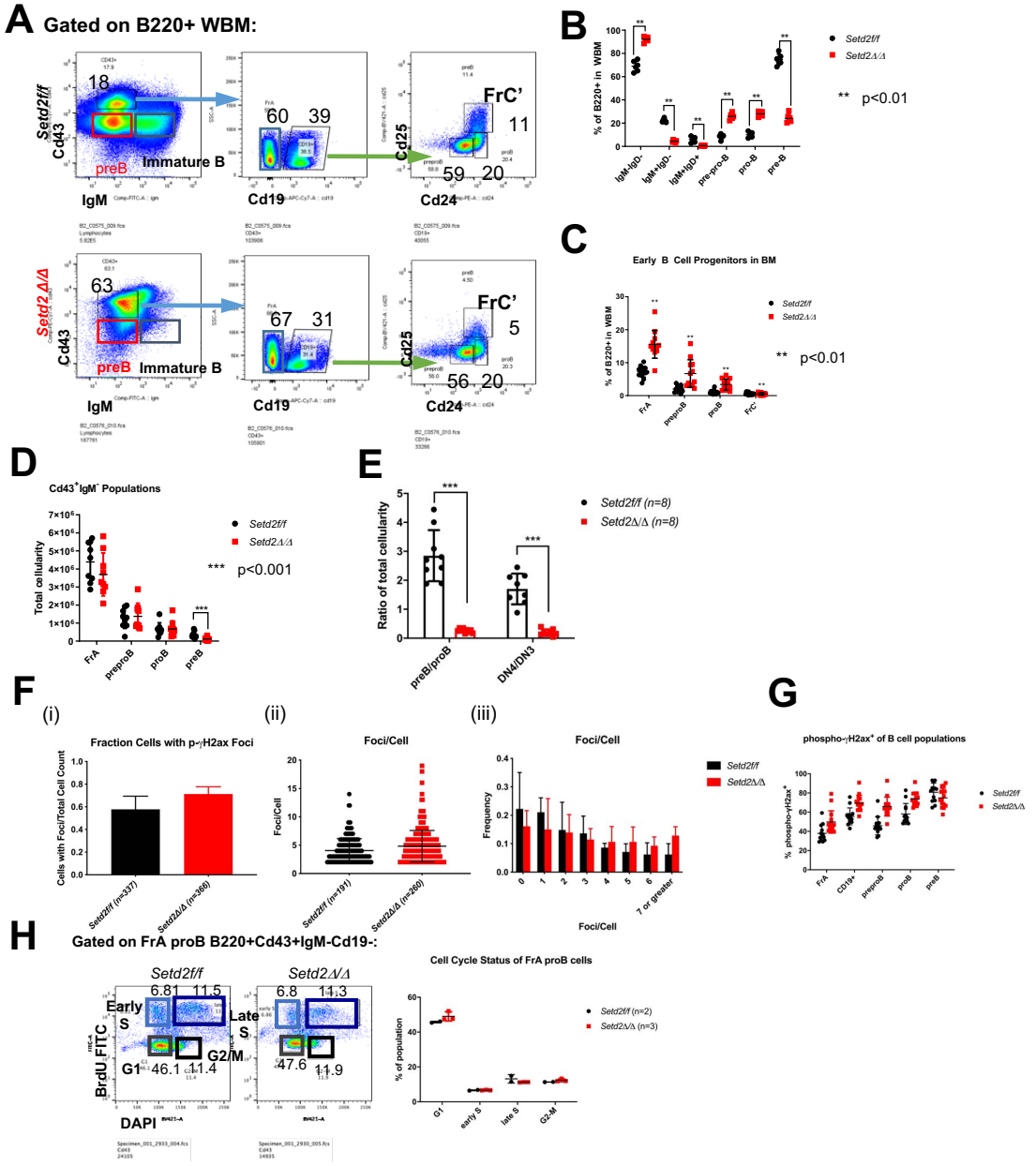

Figure S3. Loss of *Setd2*/H3K36me3 arrests development at a proB cell stage, Related to Figure 3. **(A)** Representative flow cytometry plots with gating strategy for different B cell progenitor populations for controls and *Setd2Δ/Δ* B220$^+$ BM cells. Fraction A (FrA): B220$^+$IgM$^-$Cd43$^+$Cd19$^-$Cd24^{lo}Cd25; pre-proB: B220$^+$IgM$^-$Cd43$^+$Cd19$^+$Cd24^{lo}Cd25$^-$, proB: B220$^+$IgM$^-$Cd43$^+$Cd19$^+$Cd24^{hi}Cd25$^-$; FrC': B220$^+$IgM$^-$Cd43$^+$Cd19$^+$Cd24^{hi}Cd25$^+$; preB: B220$^+$IgM$^-$Cd43$^-$; immature B: B220$^+$Cd43$^-$IgM$^+$. **(B)** Percent composition of B220$^+$ WBM of different B cell population in the bone marrow (n = 6). **(C)** B cell progenitor proportions in B220$^+$ BM of *Setd2Δ/Δ* and controls (n= 14 for all groups). **(D)** Total cellularity of B cell progenitor proportions in B220$^+$Cd43$^+$IgM$^-$ BM of *Setd2Δ/Δ* and controls. n= 9 for all groups. **(E)** Ratio of preB to proB compartment and DN4 to DN3 compartment total cellularity from BM of *Setd2Δ/Δ* and controls (n= 8 for all groups, from Fig. 3A-B) **(F)** Quantification of phospho-γH2ax foci by immunofluorescence from sorted FrA proB cells from *Setd2Δ/Δ* (n=8 mice) and controls (n=7 mice). (i) Fraction of total cells containing foci (n=366 for *Setd2Δ/Δ*, n= 337 for controls). (ii) Foci/cell in cells containing phospho-γH2ax foci (n=260 for *Setd2Δ/Δ*, n= 191 for controls). (iii) Frequency of foci/cell for all cells containing phospho-γH2ax foci for *Setd2Δ/Δ* and controls. **(G)** percent of different B cell populations positive for phospho-γH2ax by flow cytometry (n=15 for *Setd2Δ/Δ,* n=13 for controls). All groups were significant (p<0.01) except for preB population. **(H)** Representative flow cytometry plot of cell cycle status indicated by co-staining with DAPI and BrdU incorporation of sorted FrA proB cells from *Setd2Δ/Δ* (n=3) and controls (n= 2) and summary graph of each cell cycle stage. All values for cell cycle status were non-significant. **, p<0.01 ***, p<0.001, error bars represent SD.

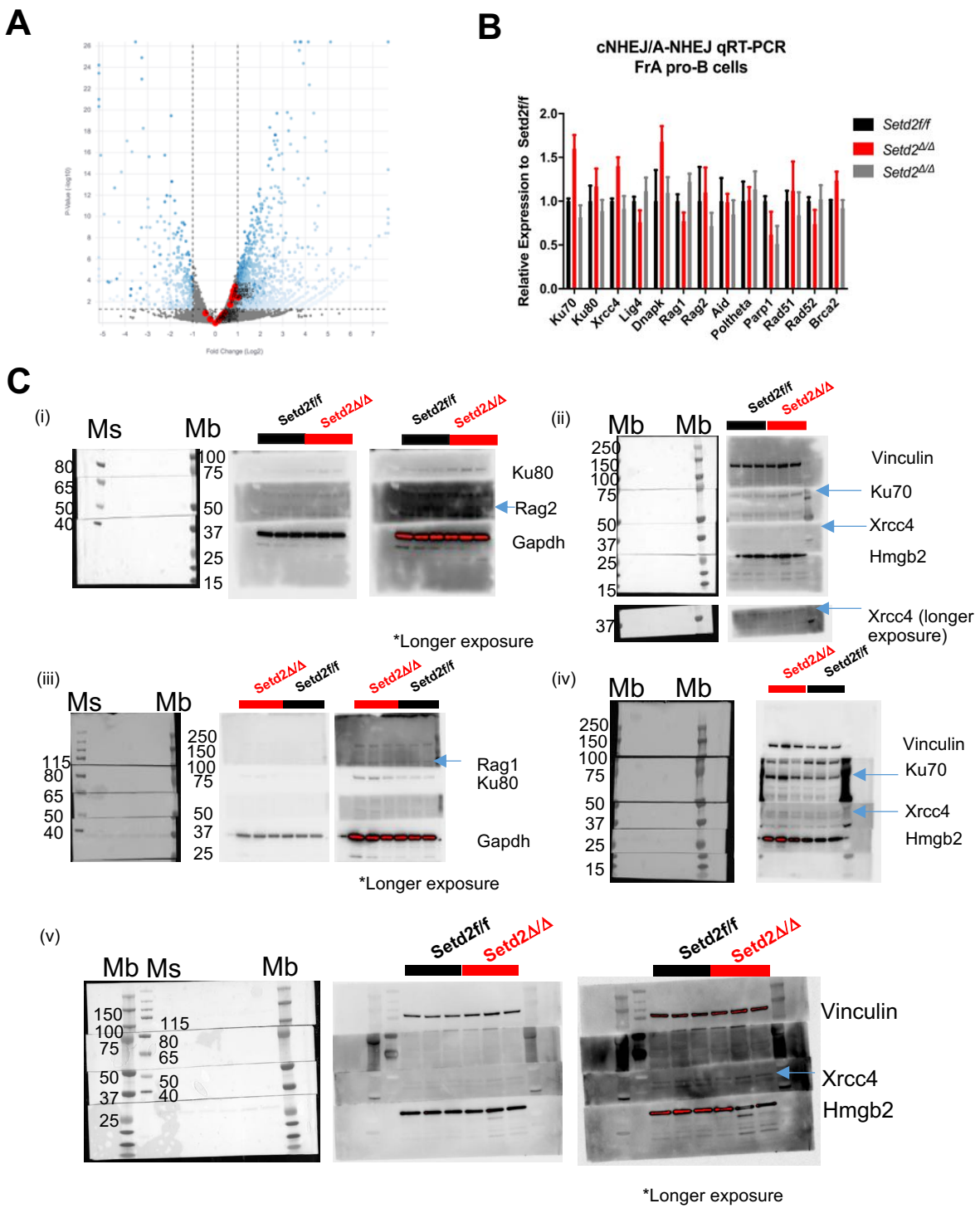

Figure S4. Loss of *Setd2*/H3K36me3 does not alter expression of C-NHEJ and A-NHEJ proteins, Related to Figure 3.

(A) Volcano plot of fold expression of a FrA proB cell compartment sorted from n=3 independent *Setd2Δ/Δ* and littermate control mice and subjected to by RNA-Sequencing. Genes highlighted include: *Rag1, Rag2, Xrcc4, Lig4, Xrcc5, Xrcc6, Xrcc7, Prkdc, Hmgb2, Mre11a, Dclre1c, Atm, Parp1, Polq, Brca2, Ctbp1, Rad52, Mrnip.* **(B)** Real-time PCR of C-NHEJ and A-NHEJ genes of FrA proB cells sorted from n=2 *Setd2Δ/Δ* mice and a littermate control. Expression was normalized to *Gapdh* expression and calculated relative to the wildtype control by a ΔΔCt method. **(C)** (i-v) Immunoblotting of FrA proB cells sorted from n=3 *Setd2Δ/Δ* mice and n=3 littermate controls (*Setd2f/f*) for C-NHEJ proteins Ku70, Ku80, Xrcc4, Rag1, Rag2, Hmgb2 with loading controls Vinculin and Gapdh. Mb – low molecular weight ladder, Ms – high molecular weight ladder.

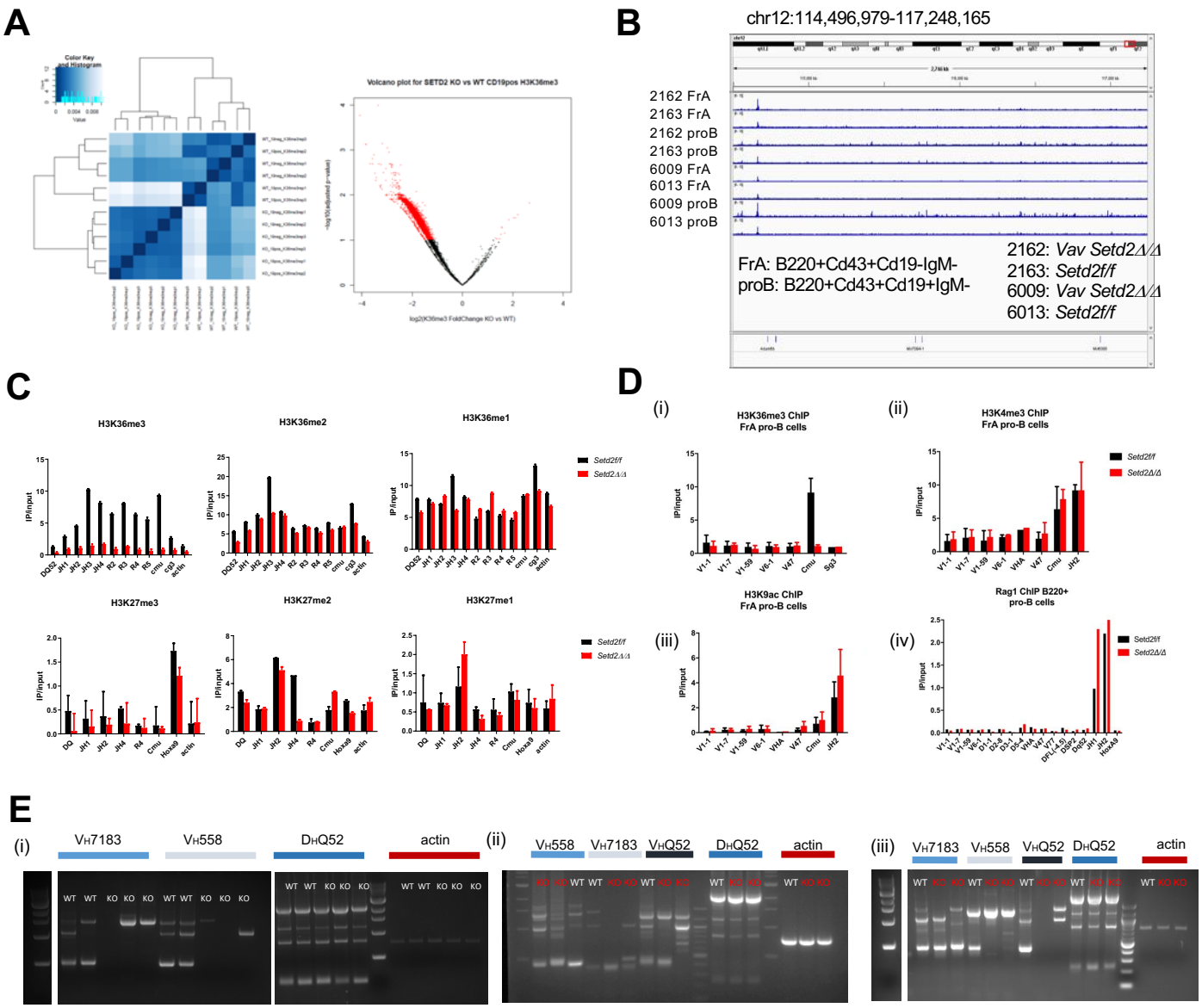

Figure S5. Loss of H3K36me3 does alter local chromatin architecture or accessibility of the *Igh* locus but leads to aberrant V(D)J recombination, Related to Figure 4.

(A) Composite Heatmap and volcano plot of H3K36me3 ChIP-Seq signal of Cd19$^-$ and Cd19$^+$ control (WT) and *Setd2Δ/Δ* (KO) proB cells (B220$^+$Cd43$^+$IgM$^-$) (n=3 for each genotype). **(B)** ATAC-sequencing tracks from Cd19$^-$ and Cd19$^+$ control (WT) and *Setd2Δ/Δ* (KO) proB cells (B220$^+$Cd43$^+$IgM$^-$) (n=2 for each genotype) across the Igh locus. **(C)** Representative ChIP-PCR of relative abundance of H3K36me1-3 and H3K27me1-3 at regulatory region of Igh locus. Regions R1-R5 were regions with H3K36me signal in between the Eμ enhancer binding site and Cμ gene region with HoxA9, Cγ3 and actin as controls. Data is representative of n = 2 independent experiments. **(D)** (i-iii) H3K36me3, H3K4me3, and H3K9ac ChIP-PCR of variable heavy chain gene families and from n=4 independent ChIP experiments and (iv) Rag1 occupancy by ChIP-PCR variable gene family genes with primers from (Ji et al 2019 and (Ji et al., 2010; Hauser et al., 2014; Subrahmanyam et al., 2012; Chakraborty et al., 2009; Hesslein, et al, 2003). (n=1 ChIP). **(E)** (i-iii) replicates of PCR assay to detect V(D)J recombination products of rearrangement shown in Figure 2E of the Igh locus of different V_H families from independently sorted proB cells from *Setd2Δ/Δ* (KO) and controls (WT). No product meant germline non-rearrangement.

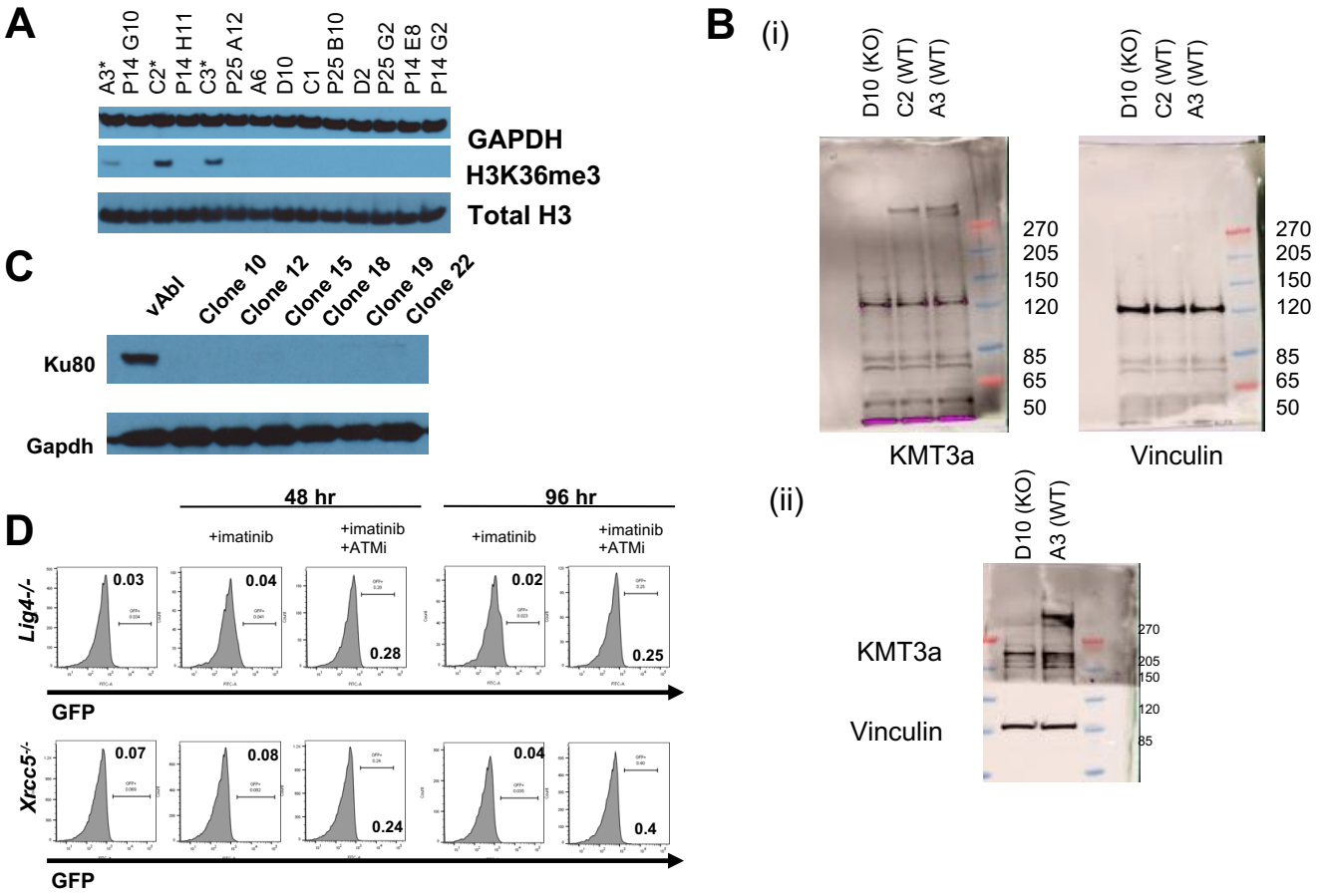

Figure S6. Generation of v-Abl transformed *Setd2, Xrcc5* and *Lig4* deficient cell lines, Related to Figure 5.

(A) H3K36me3 levels of several individual v-Abl clones (used in Figure 5) that were either *Setd2* wildtype (wt, indicated with asterisk) or *Setd2* deficient lines (*Setd2*$^{-/-}$ or KO). Total H3 and Gapdh were used as loading controls. **(B)** (i-ii) immunoblots of *Setd2* wildtype or *Setd2*$^{-/-}$ v-Abl lines for Kmt3a (Setd2) and Vinculin loading controls. **(C)** Immunoblot of v-Abl lines for *Xrcc5* (*Ku80*) null lines. Gapdh was used as a loading control. **(D)** Representative flow cytometric analysis of GFP expression in *Lig4* and *Xrcc5*$^{-/-}$ pMG-INV v-Abl cells treated with Abl kinase inhibitor imatinib (STI-571) and ATM kinase inhibitor (ATMi, KU55933) for 48 and 96 hours. Representative of 4 independent induction experiments.

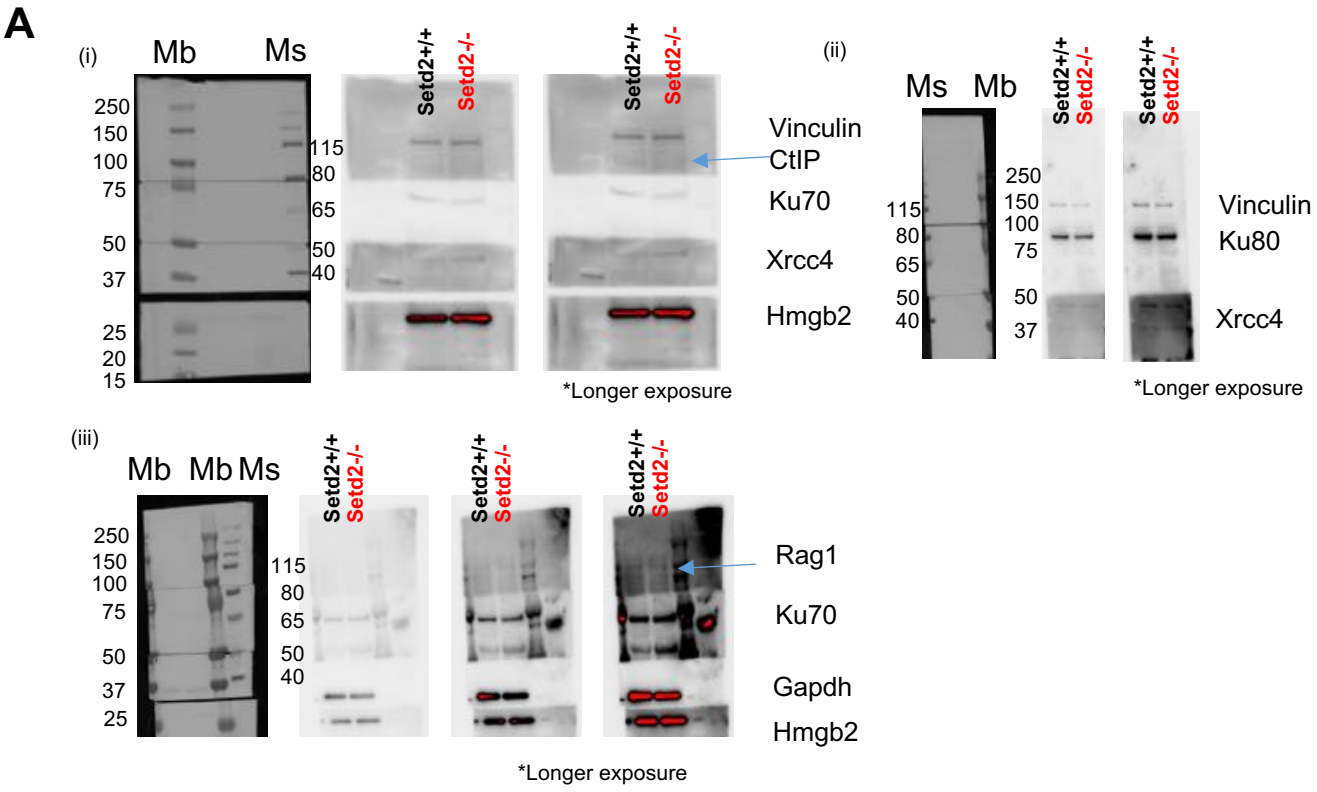

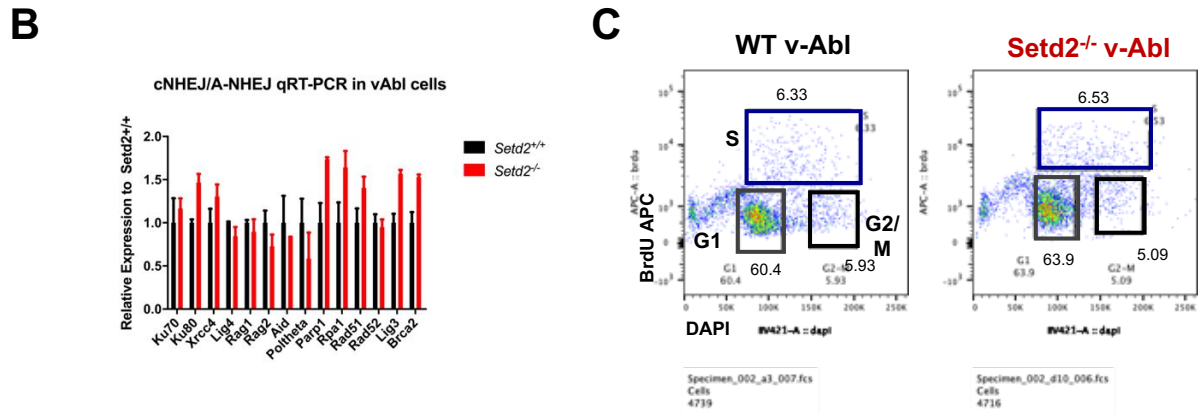

Figure S7. Deletion of *Setd2* in v-Abl cells does not alter expression of C-NHEJ and A-NHEJ proteins or cell cycle status, Related to Figure 5.

(A) (i-iii) Immunoblotting of WT and *Setd2*$^{-/-}$ v-Abl clones for C-NHEJ proteins Ku70, Ku80, Xrcc4, Rag1, Rag2, Hmgb2 with loading controls Vinculin and Gapdh. Mb – low molecular weight ladder, Ms – high molecular weight ladder. **(B)** Real-time PCR of C-NHEJ and A-NHEJ genes of *Setd2* deficient and WT v-Abl transformed cells. Expression was normalized to *Gapdh* expression and calculated relative to the wildtype control by a ΔΔCt method. **(C)** Representative flow cytometry plot of cell cycle status indicated by co-staining with DAPI and BrdU incorporation of *Setd2* deficient and WT v-Abl cells. All data representative of n=2 independent experiments. Error bars represent SD.

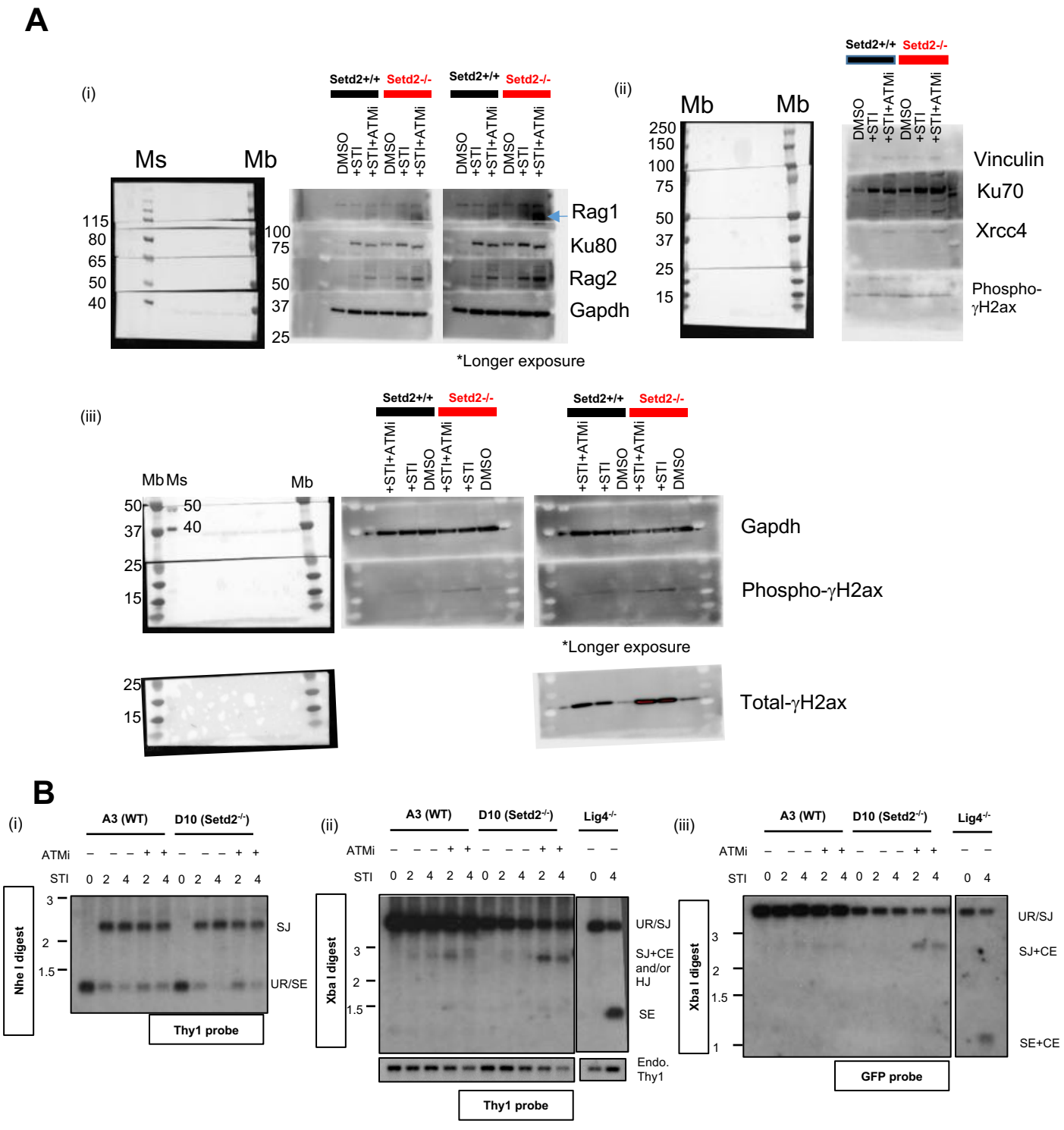

Figure S8. Dual loss of *Setd2*/H3K36me3 and Atm activity leads to abnormal recombination and end-joining repair, Related to Figure 5.

(A) (i-iii) Immunoblotting for NHEJ proteins and phospho- and total γH2ax of WT (*Setd2*$^{+/+}$) and *Setd2* deficient (*Setd2*$^{-/-}$) v-Abl cells treated for 48 hours with STI or STI+ATMi. Data representative of 3 independent induction experiments. Mb – low molecular weight ladder, Ms – high molecular weight ladder. **(B)** Replicate Southern blot analysis of genomic DNA from *Setd2*$^{-/-}$ clone (D10) and control line that were digested with NheI (left) and XbaI (middle and right panels) and hybridized with Thy1 probe (middle, right panels) or GFP probe (left panel). Bands indicated are for URs, SJs, CJs, SEs, CJ+SEs or SJ+CEs. Hybrid Joins (HJ) indicated as well. Southern blots were generated from an independent induction experiment of v-Abl clones with imatinib and ATMi shown in Figure 5.

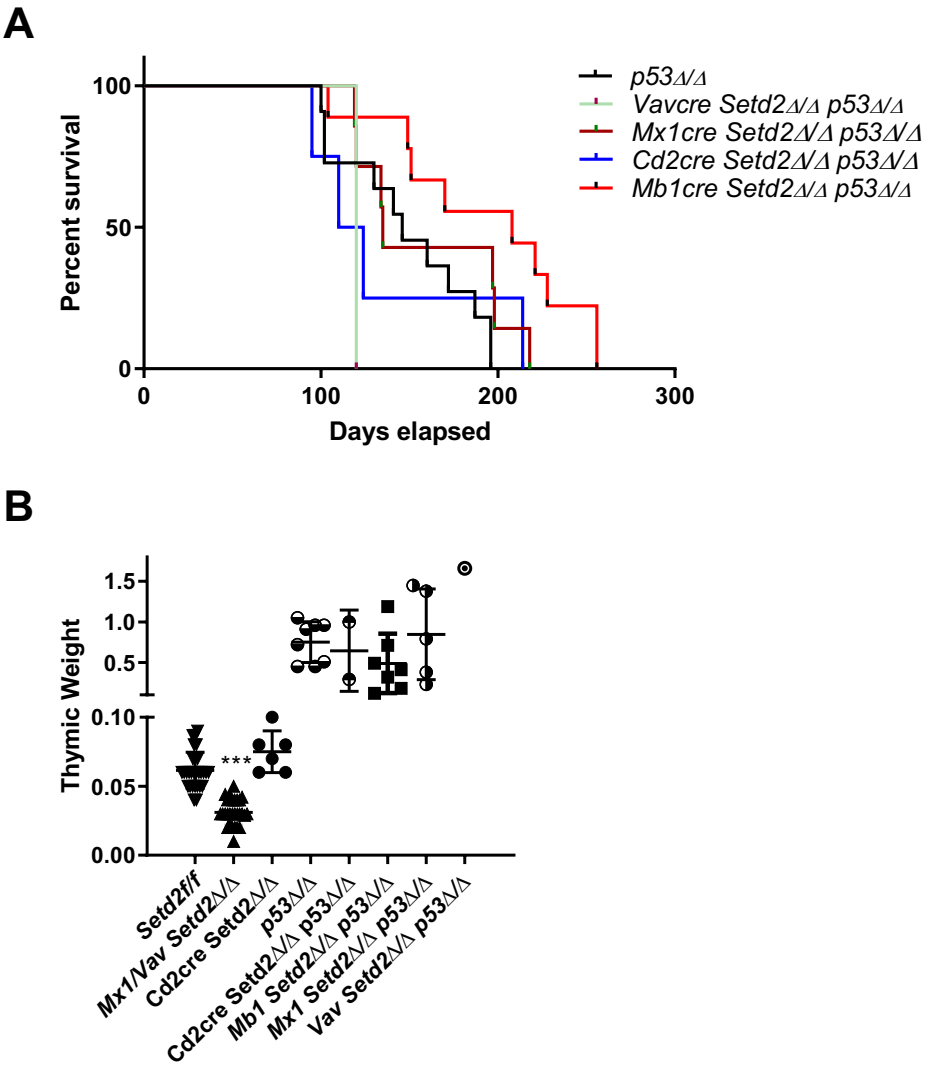

Figure S9. Dual loss of *Setd2*/H3K36me3 and p53 does not lead to the development of pro-B lymphomas, Related to Figure 5.

(A) Kaplan-Meier survival of double knockout *Vav* (n= 1), *Mx1* (n=7), *Cd2* (n=4) , *Mb1cre* (n=9) *Setd2Δ/Δ p53Δ/Δ* mice and controls (n = 11). All mice developed thymic lymphomas. **(B)** Weight of thymus in mouse thymic lymphomas from double knockout mice and controls. ***, $p<0.001$ calculated to control (*Setd2f/f* $p53^{+/+}$). Error bars represent SD.

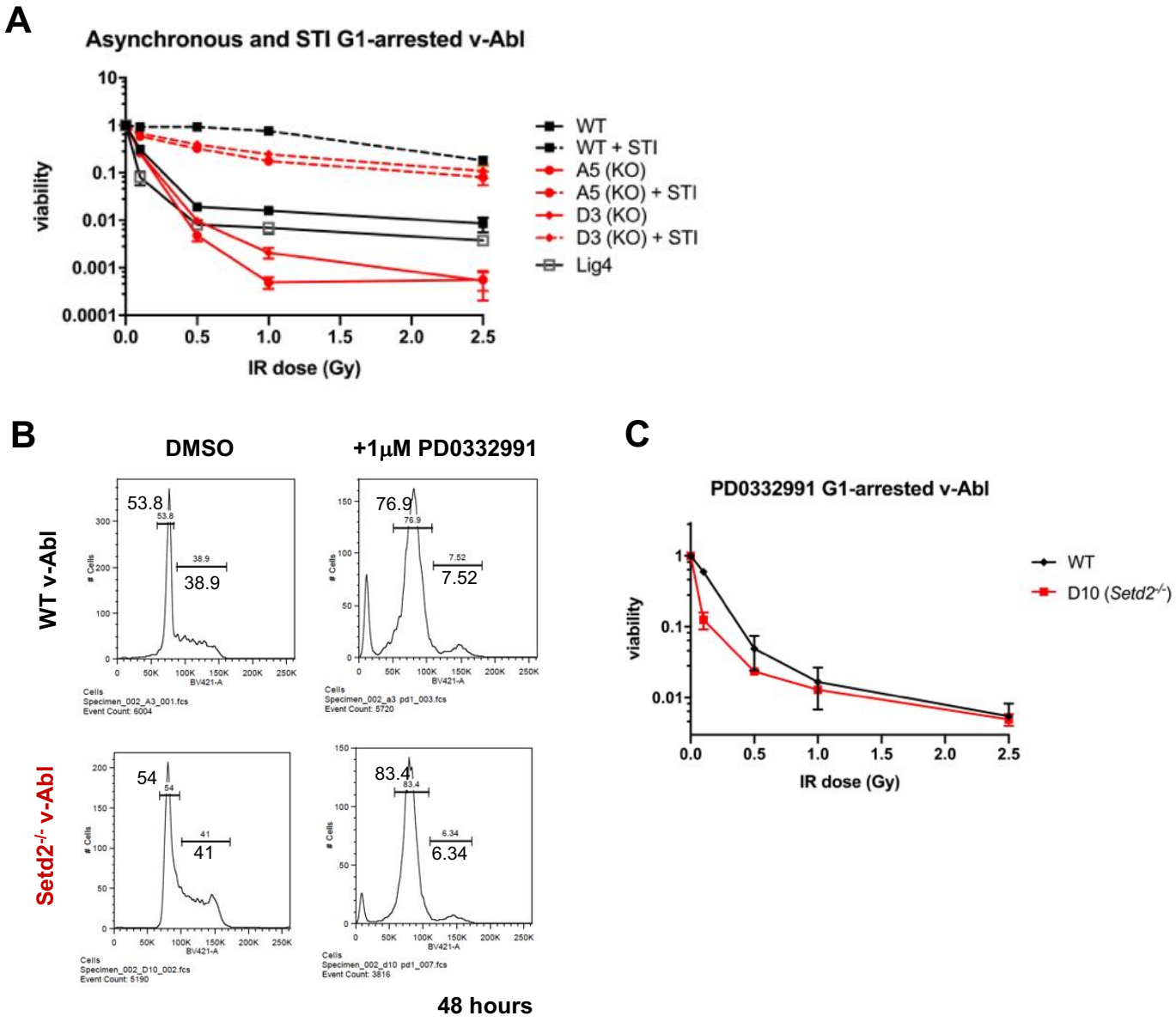

Figure S10. Asynchronous and synchronous *Setd2* deficient v-Abl cells exhibit increased sensitivity to ionizing radiation, Related to Figure 7.

(A) Asynchronous and STI G1-arrested WT, *Lig4*$^{-/-}$ and 2 different *Setd2*$^{-/-}$ v-Abl cells subjected to different doses of ionizing radiation and serially diluted 5 times in triplicate to assess survival. Values plotted as a mean of each dose as a percent of non-irradiated controls, bars represent standard deviation. Data is representative for 3 different independent treatment experiments. Viability was assessed at 72 hours. **(B)** Representative flow cytometric analysis of cell cycle status as determined by DNA content with DAPI staining 48 hours after treatment with 1mM Cdk4/6 inhibitor PD0332991. Data representative of n=3 independent experiments. **(C)** PD0332991 G1-arrested WT *Setd2*$^{-/-}$ v-Abl cells subjected to different doses of ionizing radiation and serially diluted 5 times in triplicate to assess survival. Values plotted as a mean of each dose as a percent of non-irradiated controls, bars represent standard deviation. Data is representative for 3 different independent treatment experiments. Viability was assessed at 72 hours.

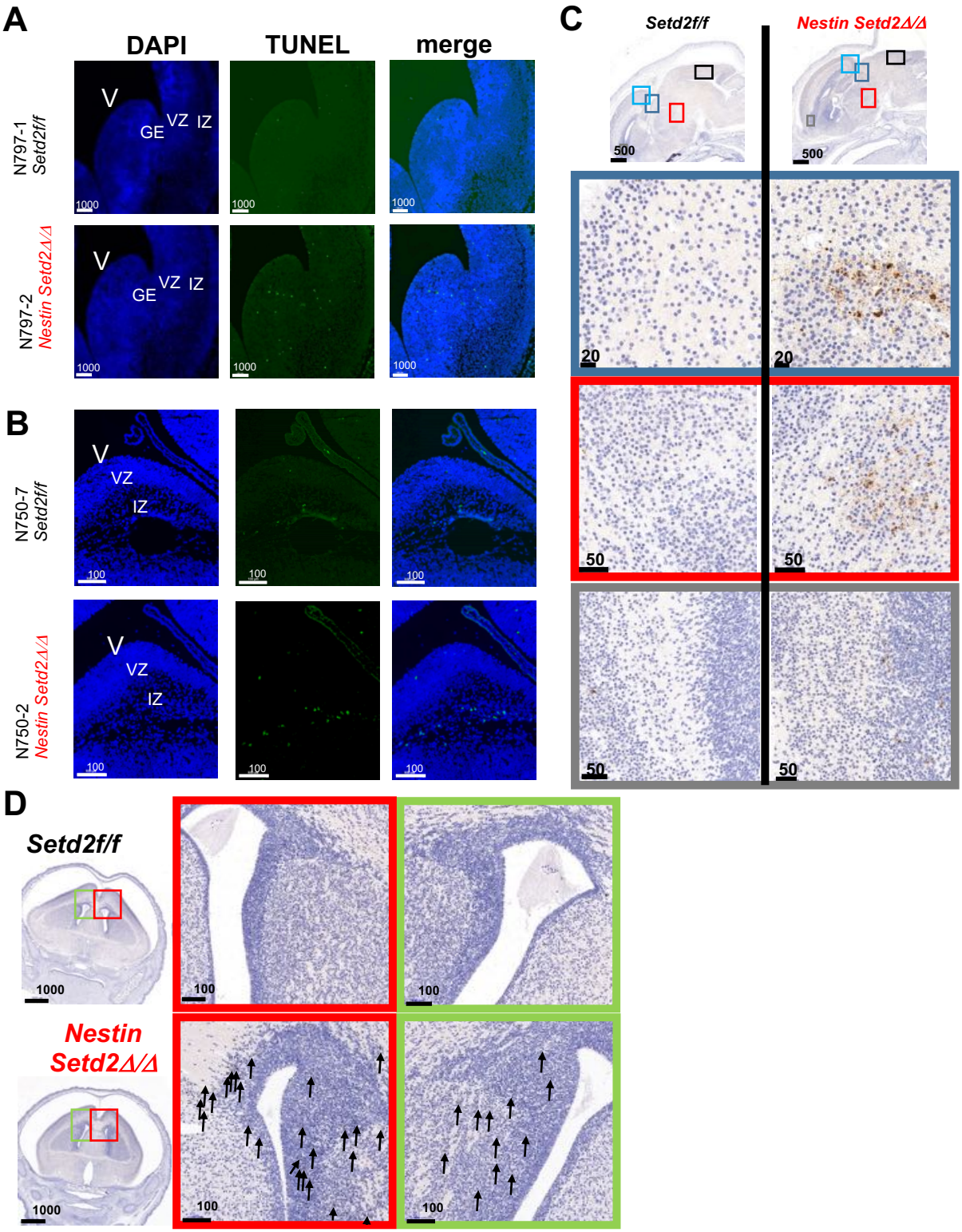

Figure S11. Post-mitotic neuronal apoptosis with loss of *Setd2*/H3K36me3, Related to Figure 7. **(A,B)** TUNEL assay of two independently matched control and *Nestin-cre Setd2Δ/Δ* E14.5 coronal sections of the lateral ventricle displaying the ganglionic eminence (GE), Lateral Ventricle (V), Ventricular zone and intermediate zone (IZ) of the telencephalon. Distances as indicated in microns. **(C)** Higher magnification of cleaved Caspase-3 immunohistochemistry of E18.5 sagittal regions of lateral ventricle of control and *Nestin-cre Setd2Δ/Δ* embryos from Figure 7D. Distances as indicated in microns. **(D)** Cleaved caspase-3 immunohistochemistry of coronal sections of the lateral ventricle of 2 hour post-partum control and *Nestin-cre Setd2Δ/Δ* pups from same samples as shown in Figure 7E. Magnifications indicated by corresponding red and green boxes. Arrows indicate cleaved caspase-3 staining and pyknotic nuclei. Distances as indicated in microns.

Transparent Methods

Mice and Isolation of primary B cells and v-Abl B cells

Strategy for generating *Setd2Δ/Δ* mice was previously described (Mar et al., 2018). *Setd2f/f* mice were bred to *Mx1, Vav1, Cd19, Mb1, hCD2-cre* mice to homozygosity. At 6-8 weeks of age, mice were sacrificed and bone marrow from femurs, tibias, hips, and spines were isolated. BM was then RBC lysed and stained with B220-biotin (BD Pharmingen) and subsequently stained with Anti-biotin microbeads (Miltenyi) and applied on a LS column (Miltenyi). Subsequent staining for cellular antigens was conducted. For V(D)J recombination product assessment, RNA-Seq, ChIP-Seq, ChIP-PCR, and qPCR were stained and sorted by FACS (BD-Aria) for $B220^{+}Cd43^{+}IgM^{-}Cd25^{-}Cd19^{-}$ proB cells and $B220^{+}Cd43^{-}IgM^{-}$ for preB. IgHelMD4 (Goodnow et al., 1988) and *Mb1cre* mice were generously provided by Jayanta Chaudhuri. All mouse experiments were approved by the Institutional Animal Care and Use Committees at Dana-Farber Cancer Institute and Memorial Sloan Kettering Cancer Center.

WT and *Lig4*$^{-/-}$ v-Abl B cell lines were generously provided by Andre Nussenzweig and Barry Sleckman (Bredemeyer et al., 2006). *Xrcc5* and *Setd2* knockout v-Abl cells were generated as before (Bredemeyer et al., 2006; Jacobsen et al., 2006). Briefly, CMV expression vectors containing Cas9 and a BFP tagged expression vector (Hung et al., 2018) with sgRNAs targeting gene of interest were nucleofected with Amaxa nucleofection Kit P4 as per manufacturer's instructions (Lonza). Less than 24 hours later, BFP^{+} cells were single cell sorted into 96 well plates and expanded and western blotting was conducted to confirm protein knockout. Single cell clones with confirmed knockout of protein were transduced with retrovirus containing pMG-INV (Hung et al., 2018) vector and subsequently sorted for expression of cell surface marker Thy1.2. The recombination substrate vector pMG-INV was generously provided by Barry Sleckman. To induce G1 arrest, cells were treated with 3μM imatinib (STI571) with or without 15 μM ATMi (KU55933) for up to 96 hours and assayed for GFP expression by flow cytometry and genomic DNA isolation for downstream PCR analysis. sgRNAs for CRISPR/Cas9 used were as follows: Xrcc5: sgXrcc5-1 (5'-GAATGATATCACTTCCGTAG-3'), sgXrcc5-2 (5'-GAGCTTGGTAAAGAAAAACG-3'), sgXrcc5-3 (5'-GTCATAAGCATATCGGACGA-3'), sgXrcc5-4 (5'-TGTCCTTAGAAGGCGAAGAC-3'), sgXrcc5-5 (5'-TGCACACAATCAGGGCGTCC-3'). Setd2: sgSetd2-1 (5'-GCATTCGCTTAATATCCCGG-3'), sgSetd2-2 (5'-GGAGTTCCCCTTATCGTGAG-3'), sgSetd2-3 (5'-TTGCTTATGATCGAATCCAA-3'), sgSetd2-3 (5'-TGCTCATGCTCAGAGTGACG-3'), sgSetd2-5 (5'-ATAATAGGGAGCCGACAGAC-3').

RNA-sequencing of LSK and proB cells

B cells were isolated as indicated above. LSKs were obtained by lineage depletion of WBM and conducted as per manufacturer's protocols with biotin-labeled antibodies for CD3, Gr1, Ter119, and B220 (BD Pharmingen) and subsequently subjected to magnetic depletion with anti-biotin microbeads and depletion on a LD column (Miltenyi). Lineage depleted cells were then stained with cKit and Sca1 and sorted on a FACS cell sorter (BD-SORP-AriaII). Qiagen RNA kits were used as per manufacturer's protocol for RNA isolation and purity was confirmed with RNA Tapestation (Illumina). RNA-seq libraries

were prepared with NEBNext UltraKits and for proB cells. For LSKs, RNA was amplified with SMARTer Ultra Low Input RNA Kit for Illumina Sequencing.

Hematopoietic Reconstitution assays
For competitive/non-competitive reconstitution assays, $1x10^6$ total, unfractionated whole BM cells of control and fully excised *Setd2* mice were injected into lethally irradiated mice (9 cGy) and bled every 4 weeks up to 16 weeks before these mice were sacrificed and hematopoietic reconstitution was assessed in the bone marrow. Non-excised *Mx1cre Setd2Δ/Δ* mice were treated with pI:pC after 8 weeks of engraftment in reconstitution assays.

BrdU incorporation assays
For *in vivo* assessment of BrdU incorporation, BrdU was injected intraperitoneally 4 hours before mice sacrificed and BrdU incorporation was assessed as per manufacturer's protocols (BD Biosciences). Recommended manufacturer's protocols were also followed for *in vitro* labelling of v-Abl cells. Cells were labelled for 2 hours before fixed and permeabilized.

Phospho-γH2ax Immunofluorescence

Cytospins of 20 000 sorted FrA proB cells were prepared at 500 rpm for 5 minutes, permeabilized and fixed in 4% paraformaldehyde/PBS at 4°C for 10 minutes. Phospho-γH2AX (Abcam) primary antibody was used at 1:500 and incubated at 4°C overnight. Secondary antibody Anti-rabbit Alexa647 (CST) was applied for 30 minutes at room temperature. DAPI (1 µg/ml) counterstaining was conducted for 5 minutes at room temperature and covered with Prolong Gold Antifade Reagent (ThermoFisher). Slides were analyzed by confocal microscopy (Leica TCS SP5) (Leica) and foci were quantified using Image J software (NIH).

Ionizing Radiation Sensitivity Assay
Ionizing radiation sensitivity assays were performed for v-Abl lines that were either asynchronous or G1 arrested with STI-571 (Selleckchem) or PD-0332991 (Sigma-Aldrich) before irradiation. Cells were treated with 0.1, 0.5, 1, or 2.5 Gy ionizing radiation with percent survival measured relative to a non-irradiated and non-treated control for each cell line assayed. Cells that were G1 arrested were treated 48 hours prior to irradiation before washing off medium containing 3μM STI571 or 1μM PD-0332991 and re-plated with fresh media. 50,000 cells were initially plated in 96 non-tissue culture treated plates and 1:1 serially diluted 5 times with 3 replicates for each condition and cultured at for 3 days. Viability was measured by staining with DAPI and measured by flow cytometry on BD Fortessa in HTS mode.

Genomic DNA isolation
Up to $5x10^6$ proB cells were harvested and genomic DNA extracted using PureLink Genomic DNA kit (Invitrogen) as per manufacturer's protocols.

PCR analyses

PCR of retroviral substrate coding joints (CJs) and hybrid joints (HJs): pMG-INV was generously provided by Barry Sleckman (Hung et al., 2018). Oligonucleotides CJ_F and CJ_HJ_R were used to amplify CJs in pMG-INV. Oligonucleotides HJ_F and CJ_HJ_R were used to amplify HJs. CJ_F: (5'-TCAGCCAGAAATTCAGTGGCA-3'); HJ_F: (5'-TTGTACACCCTAAGCCTCCG-3'); CJ_HJ_R: (5'-GCTTATCGATACCGTCGACCT-3'). All PCRs were done on genomic DNA from cells that had been treated with STI571 for 96 hours. The *Il2* gene was amplified using the IMR42 and IMR43 oligonucleotides (Bredemeyer et al., 2006). PCRs for the *Il2* gene, and all retroviral HJs and CJs, were carried out in 50µL with cycling conditions of 95ºC for 2 minutes followed by 30 cycles 94ºC 30s, 55ºC 30s, 72ºC 60s (Bredemeyer et al., 2006). Murine *Il-2*: forward (5'-CTAGGCCACAGAATTGAAAGATCT-3'); reverse (5'-GTAGGTGGAAATTCTAGCATGATGC-3')

PCR analyses of endogenous receptor gene rearrangements: PCR of Vκ6-23 HJs and CJs was carried out by amplifying 0.5µg of genomic DNA from B220 enriched splenocytes from *Setd2Δ/Δ* and *Setd2f/f* controls in 50µl with primers for amplification as follows: pκJa and pκ6a for HJ and pκJa and pκ6d for CJ. PCR conditions were 95ºC for 5 minutes followed by 17 cycles 94ºC 30s, 64ºC 30s, 72ºC 30s. Products from this reaction were amplified in 50µl using the above conditions with primers pκJa and pκ6b for HJ and pκJa and pκ6c for CJ and 25 amplification cycles oligonucleotides (Bredemeyer et al., 2006). pκ6a: (5'-TGCATGTCAGAGGGCACAACTG-3'); pκ6d: (5'-GAAATACATCAGACCAGCATGG-3'); pκ6b: (5'-CTACCAAACTTTGCAACACACAGGC-3'); pκ6c: (5'-ACATGTTGCTGTGGTTGTCTGGTG-3'); pκJa: (5'-GGAGAGTGCCAGAATCTGGTTTCAG-3').
PCR results were analyzed with high sensitivity D1000 TapeStation reagents (Agilent Technologies).

V(D)J recombination PCR: Assay was conducted as previously described (ten Boekel et al., 1995; Ehlich et al., 1994; Corcoran et al., 1998). Briefly, two rounds of PCR were conducted on 100-300ng of gDNA using forward primers amplifying V_H558, V_HQ52, V_H7183 family genes with nested primers located in the J_H4 gene segment. Products were visualized on a 1% agarose gel and the V-(D)J_H4 recombination product was gel extracted (Qiagen) and submitted for NGS sequencing. Vh7183_F1: (5'-CTCGCCATGGACTTCGGGTCAGTTGG-3'); Vh7183_F2: (5'-CAGCTGGTGGAGTCTGGGGGAGGC-3'): Vh558_F1: (5'-ACCATGGGATGGAGCTGKATCWTBC-3'): Vh558_F2: (5'-GTGARGCCTGGGRCTTCAGTGAAG-3'); VhQ52F: (5'-GCGAAGCTTCTCACAGAGCCTGTCCATCAC-3'): Vh7183: (5'-GCGAAGCTTGTGGAGTCTGGGGGAGGCTTA-3'); DhQ52_F1: (5'-CACAGAGAATTCTCCATAGTTGATAGCTCAG-3'); DhQ52I_F2: (5'-GCCTCAGAATTCCTGTGGTCTCTGACTGGT-3'); Jh4_R1: (5'-AGGCTCTGAGATCCCTAGACAG-3'); Jh4_R2: (5'-GGGTCTAGACTCTCAGCCGGCTCCCTCAGGG-3'); actin_738: forward (5'-GGTGTCATGGTAGGTATGGGT-3'), reverse (5'-CGCACAATCTCACGTTCAG-3').

Chromatin Immunoprecipitation (ChIP) and ChIP-sequencing

Chromatin immunoprecipitation was coupled with high-throughput sequencing (ChIP-seq). 0.5-2x10^6 primary sorted proB cells were crosslinked with 1% formaldehyde for 10 minutes followed by 0.125 M glycine for 5 minutes. Fixed cells were washed twice with ice-cold phosphate-buffered saline and resuspended in ChIP lysis buffer and sheared using a Covaris E220 ultrasonicator (Covaris). Sheared chromatin was incubated overnight at 4^{o}C with rabbit polyclonal anti-H3K36me3 (61101 pAb, Active Motif). Immune complexes were collected with protein A/G dynabeads (Invitrogen) and washed sequentially in low-salt wash buffer (20 mM Tris pH 8.0, 150 mM NaCl, 0.1% SDS, 1% Triton X-100, 2mM EDTA), high-salt wash buffer (20 mM Tris pH 8.0, 500 mM NaCl, 0.1% SDS, 1% Triton X-100, 2mM EDTA), LiCl wash buffer (10 mM Tris pH 8.0, 250 mM LiCl, 1% NP-40, 1% sodium deoxycholate, 1 mM EDTA), and TE. Chromatin was eluted buffer (1% SDS, 0.1 M NaHCO3), and then reverse cross-linked with 0.2 M NaCl at 65o C overnight. DNA was purified with a PCR purification kit (QIAGEN) and subjected to quantitative PCR or processed for ChIP-sequencing.

ChIP-PCR oligonucleotides used in this study were as follows (Ji et al., 2010; Hauser et al., 2014; Subrahmanyam et al., 2012; Chakraborty et al., 2009; Hesslein, et al, 2003):

Vha: forward (5'-CCTTCGCCCCAATCCACC-3'), reverse (5'-CAAGTAACCCTCAAGAGAATGGAGACTC-3'); Vh47: forward (5'-CTACAACCAGAAGTTCAAGGGCAA-3'), reverse (TCAGGCTGTGATTACAACACTGTGT-3'); Vh77: forward (5'-AAATCCTCCAGCACAGCCTA-3'), reverse (5'-TAGACCGCAGAGTCCTCAGA-3'); Dsp2: forward (5'- CAACAAAAACCCAGTATGCCCAG-3'), reverse (5'-GTGCTTTCACCTGTCTGTGGG-3'); Dfl-4.5: forward (5'-AGGCATCTCATCTCACTCTAAGC -3'), reverse (5'-TGTGTCCCTCTAAGACGAGTGAAT -3'); Dq52: forward (5'-CATTGGTCCCTGACTCAAGA-3'), reverse (5'-TCCCAGTTAGCACTGTGGTG-3'); Jh1: forward (5'-TGCTACTGGTACTTCGATGTCTG-3'), reverse (5'-GCCAGCTTACCTGAGGAGAC-3'); Jh2: forward(5'-CAGTCTCCTCAGGTGAGTCCT), reverse (5'-CCCAATGACCCTTTCTGACT-3'); Jh3: forward (5'-GCCTGGTTTGCTTACTGG-3'), reverse (5'-GACAAAGGGGTTGAATCT-3'); Jh4: forward (5'-CACCAGGAATTGGCATAA-3'), reverse (5'-CCTGAGGAGACGGTGACT-3'); Sμ: forward (5'-GCTAAACTGAGGTGATTACTCTGAGGT-3'), reverse (5'-GTTTAGCTTAGCGGCCCAGCTCATTCC-3'); Cμ: forward (5'-ATGTCTTCCCCCTCGTCTCC-3'), reverse (5'-TACTTGCCCCCTGTCCTCAG-3'); Sγ3: (5'-AATCTACAGAGAGCCAGGTGG-3'), reverse (5'-TGGTTTTCCATGTTCCCACTT-3');

Cγ: forward (5'-TGGACAAACAGAAGTAGACATGGGTC-3'), reverse (5'-GGGGTTTAGAGGAGAGAAGGCAC-3');

γ-actin: forward (5'-GACACCCAACCCCGTGACG-3'), reverse (5'-GCGGCCATCACATCCCAG-3');

IgHK36me3R1: forward (5'-TGGTTTCGGAGAGGTCCAGA-3'), reverse (5'-GTAGGCCTGGACTTTGGGTC-3'); IgHK36me3R2: forward (5'-CAAGCCCAGCTTTGCTTACC-3'), reverse (5'-CTGAGATGGGTGGGCTTCTC-3'); IgHK36me3R3: forward (5'-AGGGCTCTCAACCTTGTTCC-3'), reverse (5'-AGGTCGGCTGGACTAACTCT-3'); IgHK36me3R4: forward (5'-

TCTGGCTTACCATTTGCGGT-3'), reverse (5'-TCGGTGGCTTTGAAGGAACA-3'); IgHK36me3R5: forward (5'-TGGCAGAAGCCACAACCATA-3'), reverse (5'-CCCTCTGGCCCTGCTTATTG-3'); Hoxa9: forward (5'-GGAATAGGAGGAAAAAACAGAAGAGG-3'), reverse (5'TGTATGAACCGCTCTGGTATCCTT-3').
The following variable region ChIP-PCR primers were used for variable region were from (Ji et al 2019): V1-1: forward (5'- ACGTCACAGTGAGGATGTGACA-3'), reverse (5'- CTAGGCACATATCCTCCAGCAT-3'); V1-7: forward (5'-TCATCAAGCCTACAGGTTAGTC-3'), reverse (5'- AGACACAGTGGTGCAACCACAT-3'); V1-59: forward (5'- CATACTACACACCATCCTGGCT-3'), reverse (5'-AACCCTGGAGGAGTAGCAAACT-3'); V6-1: forward (5'-CTTCCTACACAAGCCATGGGTA-3'), reverse (5'- GCAACATGTTATGGAGGTTTGT-3'); D1-1: forward (5'- CTAGACTCAGTTTTTGGAGCTCAA-3'), reverse (5'-CTACGGTAGTAGCTACCACAGT-3'); D2-8: forward (5'-CTGTGGTAGTTACCATAGTAGAC-3'), reverse (5'-CTCTGGCCCCACCAGACAAT-3'); D3-1: forward (5'- AAAGCCAGAAAGGGAATAGGTCT-3'), reverse (5'-CTGTCACAGTGGGCACAGCT-3'); D5-4: (5'-CTGACTGGCTAAACACTGTAGA-3'), reverse (5'-CACAAGAGGTGGATTCTGTATGT-3'); J2: forward (5'-GAGGTTGTAAGGACTCACCTGA-3'), reverse: (5'-ACATTGTTAGGCTACATGGGTAGA-3'); J3: forward (5'-CTGCAGAGACAGTGACCAGAGT-3'), reverse (5'-TGGAGCCCTAGCCAAGGATCA-3')

For ChIP-Sequencing libraries were prepared using a ThruPLEX DNA-seq Kit (Rubicon Genomics) and validated using a TapeStation (Agilent Technologies) and Qubit 2.0 Flurometer (Thermo Fisher Scientific). Libraries were pooled and sequenced on a HiSeq2000 platform (Illumina).

Quantitative PCR
RNA isolated from sorted B cell populations and v-Abl cells were subjected to quantitative PCR with the following primers and normalized to *Gapdh* expression: From (Chakraborty et al., 2009): Dfl-4.5: forward (5'-AGGCATCTCATCTCACTCTAAGC-3'), reverse (5'-TGTGTCCCTCTAAGACGAGTGAAT-3'); Dq52: forward (5'-TGGTGCAAGGTTTTGACTAAGC-3'), reverse (CCAAACAGAGGGTTTTTGTTGAG-3'); Dsp2: forward (5'-TGTTACCTTACTTGGCAGGGATTT-3'), reverse (5'-TGGGTTTTTGTTGCTGGATATATC-3'); γ-actin: forward (5'-GGTGTCCGGAGGCACTCTT-3'), reverse (5'-TGAAAGTGGTCTCATGGATACCA-3'); Cμ: forward (5'- AGAGATCTGCATGTGCCCATT-3'), reverse (5'-TGGTGGGACGAACACATTTACA-3'); Eμ (5'): forward (5'-CTGACATTACTTAAAGTTTAACCGAGG-3'), reverse (5-CTCCAACTCAACATTGCTCAATTC-3');
Eμ(3'): forward (5'-ATTCAGCCGAAACTGGAGAGGTC-3'), reverse (5'-GGGGAAACTAGAACTACTCAAGC-3');
From Zan et al 2017: Aicda: forward (5'-AGAAAGTCACGCTGGAGACC-3'), reverse (5'-CTCCTCTTCACCACGTAGCA-3'); Rad52: forward (5'-

AGCCAGTATACAGCGGATGAA-3'), reverse (5'-GCCATGCGGCTGCTAATGTA-3'); Polθ: forward (5'-TGGCTATATGGGCAGCACCT-3' 5'-CAGAGCAATGCCCTTGGATTT-3'); Ku70: forward (5'-CACCAAGCGGTCTCTGACTT-3'), reverse (5'-AGAGAGGGCCTCAGGTAGTG-3'), Ku80: forward (5'-AGGCCCAGGAAGCTCTATCA-3'), reverse (5'-GCACTCTTGGATTCCCCACA-3'); Gapdh: forward (5′-TTCACCACCATGGAGAAGGC-3′), reverse (5′-GGCATGGACTGTGGTCATGA-3′)
Gapdh: forward (5'-CAAGCAGATGATGTTTCCTGTCC-3'), reverse (5'-AGAACTAAGGGTGGGTGGTGTAGC-3') (Wu et al., 2003).
Lig4: forward (5'-TCTGCCTTTAAGCCAATGCT-3'), reverse (5'-GTGAGAGAGCCTTCCTGTGG-3'); Xrcc4: forward (5'-TGTGTGAGTGCCAAAGAAGC-3'), reverse (5'-TCATCGGTGCTTCCATCATA-3') (Okamura et al., 2016); Lig3: forward (5'-CCTCTCCAAGCTCACCAAAG-3'), reverse (5'-TGCTCATTGTGAAGGACTCG-3');
Parp1: forward (5'-GCAGCGAGAGTATTCCCAAG-3'), reverse (5'-CCGTCTTCTTGACCTTCTGC-3') (Meador et al, 2008); Rag1: forward (5'–TGCAGACATTCTAGCACTCTGG–3'), reverse (5' ACATCTGCCTTCACGTCGAT–3');
Rag2: forward (5'-CACATCCACAAGCAGGAAGTACAC–3'), reverse (5'-CCCTCGACTATACACCACGTCAA–3') (Bender et al. 2004);
Rad51: (5'-CTCATGCGTCAACCACCAG-3'), reverse (5'-GCTTCAGGAAGACAGGGAGAG-3') (Pandit et al., 2012).

ATAC-sequencing

ATAC-seq was performed as previously described (Buenrostro et al., 2013). For each sample, cell nuclei were prepared from $5x10^4$ cells and incubated with 2.5 µL transposase (Illumina) in a 50 µL reaction for 30 minutes at 37°C. Following purification of transposase-fragmented DNA, the library was amplified by PCR and subjected to high-throughput sequencing on the HiSeq 2000 platform (Illumina).

NGS Data analysis and statistical methods

Reads from ChIP-seq and ATAC-seq libraries were trimmed for quality using 'trim_galore' and aligned to mouse genome assembly mm9 with bowtie2 using the default parameters and duplicates removed with the Picard tool MarkDuplicates (http://broadinstitute.github.io/picard/). Density profiles were created by extending each read to the average library fragment size for ChIP and 0 bp for ATAC, then computing density using the BEDTools suite (http://bedtools.readthedocs.io). Enriched regions were discovered using MACS (v1.4) and scored against matched input libraries (fold change > 2 and p-value < 1e-5). Genome browser tracks and read density tables were normalized to a sequencing depth of ten million mapped reads.

ChIP and immunoblotting antibodies

Whole cell extracts for immunoblotting and Chromatin Immunoprecipitations were conducted with H3K36me3 (61101 pAb, Active Motif), H3K36me3 (ab9050 Abcam), H327me1 (61015 Active Motif), H3K27me2 XP (D18C8, CST), H3K9ac (ab4441, Abcam), Hmgb2 (ab67282, Abcam), H3K27me3 (07-449, Millipore), H3K36me 1 (Ab9048, Abcam), H3K36me2 (ab9049, Abcam), H3K4me3 (Ab8580, Abcam), Rag1

(NBP1-74190, Novus), total H3 (Ab61251, Abcam), Ku80 (2753, CST), Gapdh (14C10, CST), Kmt3a (ab31358, Abcam), Xrcc4 (PA-76068, ThermoFisher), Rag2 (ab133609, Abcam), Ku70 (N3H10, ThermoFisher), Lig4 (ab26039, Abcam), phospho-γH2Ax (ab11174, Abcam), total H2Ax (7631 ,CST), Vinculin (4650, CST).

Southern Blot analyses

Southern blot analyses were conducted as described previously (Bredemeyer et al., 2006; Hung et al., 2018). Briefly, 10μg of genomic DNA from v-Abl B cells containing the pMG-INV recombination substrate were digested with XbaI or NheI and hybridized to a P^{32}-labeled probe for Thy1 or GFP. Thy1 and GFP probes were made from 800bp and 700bp cDNA fragments respectively. After incubating with Thy1 probe, XbaI digested Southern blots were stripped and re-probed with the GFP probe.

Detection of Igh CDR3 sequences from NGS of proB genomic DNA

MiXCR v2.1.11 (Bolotin et al., 2017) was used to detect Igh CDR3 sequences from the next generation sequencing data. Only the best matched V/D/J genes were kept for each CDR3 sequences. The unproductive CDR3s, which are out of frame or contain stop codons, were excluded from the downstream analysis. The number of N-nucleotide additions and total deletions were evaluated based on the refPoints column in MiXCR output file. Wilcoxon rank sum test was used to compare the difference for the number of CDR3 sequences, the length of CDR3 amino acid sequences, the number of N-nucleotide additions and total deletions between knockout (KO) and WT group. All the statistical tests were implemented using R.

RNA-seq data processing for TRUST

RNA-seq fastq files were aligned to mouse reference genome mm10 using STAR2 (Dobin et al., 2013). TRUST v3.0.2 (Li et al., 2017; Hu et al., 2018; Hu et al., 2019) was used to infer both partial and complete BCR CDR3 sequences and gene coverage from the aligned RNA-seq BAM files. For each RNA-seq sample, the B cell percentage was estimated by the number of reads mapped to Igh gene region divided by the number of total sequencing reads and the BCR diversity was evaluated by the normalized unique Igh CDR3 calls (Hu et al., 2019).

Generation, analysis and histology of embryos for neurogenesis

C57Bl6 *Setd2f/f* mice were bred to *Nestin-cre* mice to heterozygosity and timed matings between *Setd2f/f* and *Nestin Setd2Δ/+* were established to obtain E14.5, E16.5, E18.5 embryos and 2 hour post-partum pups. Tissues were fixed in 10% buffered formalin and embedded in paraffin and serially sectioned for sagittal and coronal sections (4 μm). TUNEL was performed on sections using TUNEL In Situ Cell Death Detection kit, POD (Roche) with Terminal Deoxynucleotidyl Transferase buffer (Takara Bio) and counterstained with DAPI. Immunostaining of cleaved caspase-3 was performed using anti-cleaved caspase-3 (Asp175) (5A1E) (CST 9664) with anti-rabbit conjugated to HRP secondary antibodies and visualized with DAB. Nuclei counterstained with hematoxylin. Whole tissues on slides were scanned by a digital slides scanner (3D Histech, MIDI) and viewed with Caseviewer (3D Histech).

Statistical analyses

Error bars in all data shown represent standard deviation. Unless otherwise indicated, determination of statistical significance and standard deviations were calculated using unpaired two-tailed Student's t test (when comparing two conditions e.g. control vs knockout) or one way ANOVA (when comparing across multiple conditions concurrently) using Prism 7 software (GraphPad).

Supplementary References

Bender, T.P., Kremer, C.S., Kraus, M., Buch T., and Rajewsky, K. (2004). Critical Functions for c-Myb at Three Checkpoints During Thymocyte Development. *Nat Immunol*. 5:721-9. doi: 10.1038/ni1085.

ten Boekel, E., Melchers, F., Rolink, A. (1995). The status of Ig loci rearrangements in single cells from different stages of B cell development. *International Immunology*. **7**, 1013-1019. doi:10.1093/intimm/7.6.1013.

Buenrostro, J.D., Giresi, P.G., Zaba, L.C., Chang, H.Y., and Greenleaf, H.Y. (2013). Transposition of native chromatin for fast and sensitive epigenomic profiling of open chromatin, DNA-binding proteins and nucleosome position. *Nat Methods*. doi: 10:1213-1218. doi:10.1038/nmeth.2688.

Corcoran, A., Riddell, A., Krooshoop, D., and Venkitaraman, A.R. (1998). Impaired immunoglobulin gene rearrangement in mice lacking the IL-7 receptor. *Nature*. 26:904-907. doi:10.1038/36122.

Deriano, L. and Roth, D.B. (2003). Modernizing the nonhomologous end-joining repertoire: alternative and classical NHEJ share the stage. *Annu Rev Genet.* 47:433–455. doi: 10.1146/annurev-genet-110711-155540.

Dobin, A., Davis, C.A. Schlesinger, F., Drenkow, J., Zaleski, C., Jha, S., Batut, P., Chaisson, M., and Gingeras, T.R. (2013). STAR: ultrafast universal RNA-seq aligner. *Bioinformatics.* 29:15–21. doi:10.1093/bioinformatics/bts635.

Ehlich, A., Martin, V., Müller, W., and Rajewsky, K. (1994). Analysis of the B-cell progenitor compartment at the level of single cells. *Curr Biol*. 4:573-583.

Goodnow, C.C., Crosbie, J., Adelstein, S., Lavoie, T.R., Smith-Gill, S.J., Brink, R.A., Pritchard-Briscoe, H., Wotherspoon, J.S., Loblay, R.H., Raphael, K., et al. (1988). Altered immunoglobulin expression and functional silencing of self-reactive B lymphocytes in transgenic mice. *Nature*. 334: 676-82. doi:10.1038/334676a0.

Hauser, J., Grundstrom, C., and Grundstrom, T. (2014). Allelic Exclusion of IgH through Inhibition of E2A in a VDJ Recombination Complex. *J Immunol*. 192:2460-2470. doi: 10.4049/jimmunol.1302216.

Hesslein, D.G.T., Pflugh, D.L., Chowdhury, D., Bothwell, A.L.M., Sen, R., and D.G. Schatz. (2003). Pax5 is required for recombination of transcribed, acetylated, 5′ IgH V gene segments. *Genes Dev.* 7: 37–42. doi: 10.1101/gad.1031403.

Meador, J.A., Zhao, M., Su, Y., Narayan, G., Geard, C.R., and A.S. Balajee. (2008).

Histone H2AX is a critical factor for cellular protection against DNA alkylating agents. *Oncogene*. 27:5662-5671. doi: 10.1038/onc.2008.187.

Okamura, K. and Nohara, K. (2016). Long-term Arsenite Exposure Induces Premature Senescence in B Cell Lymphoma A20 Cells. *Arch Toxicol.* 90: 793-803. doi: 10.1007/s00204-015-1500-2.

Pandit, S.K., Westendorp, B., Nantasanti, S., Liere, E., Tooten, P.C.J., Cornelissen, P.W.A., Toussaint, M.J.M., Lamers, W.H. and Bruin, A. (2012). E2F8 Is Essential for Polyploidization in Mammalian Cells. *Nat Cell Biol.* 14:1181-91. doi: 10.1038/ncb2585.

Subrahmanyam, R., Du, H., Ivanova, I., Chakraborty, T., Ji, Y., Zhang, Y., Alt, F.W., Schatz, D.G., and Sen, R. (2012). Localized epigenetic changes induced by DH recombination restricts recombinase to DJH junctions. *Nat. Immunol*. 13:1205–1212. doi: 10.1038/ni.2447.

Wu, K., Jiang, S., and Couch, F.J. (2003). p53 Mediates Repression of the BRCA2 Promoter and Down-Regulation of BRCA2 mRNA and Protein Levels in Response to DNA Damage. *J Biol Chem.* 278: 15652-60. doi: 10.1074/jbc.M211297200.

Zan, H., Tat, C., Qiu, Z., Taylor, J.R., Guerrero, J.A., Shen, T., and Casalib, P. (2017). Rad52 competes with Ku70/Ku86 for binding to S-region DSB ends to modulate antibody class-switch DNA recombination. *Nat Commun*. 8:14244. doi: 10.1038/ncomms14244.